LATE CENOZOIC HIGH-ANGLE TRANSTENSIONAL AND LOW-ANGLE DETACHMENT FAULTS IN THE EASTERN MINA DEFLECTION, WEST-CENTRAL NEVADA

by

Brent Cland

APPROVED BY SUPERVISORY COMMITTEE:

_____

Dr. John S. Oldow, Chair

_____

Dr. Tom H. Brikowski, Co-Chair

_____

Dr. William R. Griffin

LATE CENOZOIC HIGH-ANGLE TRANSTENSIONAL AND LOW-ANGLE DETACHMENT FAULTS IN THE EASTERN MINA DEFLECTION, WEST-CENTRAL NEVADA

by

BRENT CLAND, B.S

THESIS

Presented to the Faculty of

The University of Texas at Dallas

in Partial Fulfillment

of the Requirements

for the Degree of

MASTER OF SCIENCE IN

GEOSCIENCES

THE UNIVERSITY OF TEXAS AT DALLAS

August 2018

ACKNOWLEDGEMENTS

I would like to thank Dr. John S. Oldow for his mentorship, contributions and assistance throughout this research project. I would also like to thank my committee members, Dr. Tom Brikowski and Dr. Randy Griffin, for their feedback and comments on this research. I give many thanks to my parents and my brother Patrick Cland, and to my colleagues Nick Mueller and David Katopody for their continued support and advice throughout my graduate studies. I would like to give a special thanks to Scott Kerstetter for his mentorship and contributions to this research, and his assistance in building an understanding of the structure and stratigraphy of the Mina deflection area. Additionally, I would like to thank August Ridde for his assistance in generating the ArcGIS shapefiles for topographic contours on the geologic maps included in this thesis. This research was supported by the National Science Foundation (EAR-0948542 and EAR-1318727), Pioneer Natural Resources, and the Ellison Miles Foundation.

July 2018

ABSTRACT

LATE CENOZOIC HIGH-ANGLE TRANSTENSIONAL AND LOW-ANGLE DETACHMENT FAULTS IN THE EASTERN MINA DEFLECTION, WEST-CENTRAL NEVADA

Brent Cland, M.S.
The University of Texas at Dallas, 2018

Supervising Professor: Dr. John S. Oldow

The region in west-central Nevada underlain by the Mina deflection, a belt of curved east-northeast and north-northwest high-angle faults linking the Eastern California Shear Zone and southern Walker Lane to the central Walker Lane, records late Cenozoic extension on a low-angle detachment fault system and superposed high-angle faults. The northern Silver Peak and Monte Cristo Ranges, the southern Cedar Mountains, and Royston Hills of the eastern Mina deflection expose a belt of east-northeast left-oblique faults that curve around deep prismatic basins emerging as north-northwest right-oblique faults. The array of curved faults underlies an east-northeast-trending region 120 km long and 50 km wide, that is characterized by well-developed scarps in alluvium and bedrock. The faults have displacements that reflect transtensional deformation that was initiated between 3 to 5 Ma. These pervasive structures are superposed onto a previously unrecognized, regionally extensive detachment fault system, the

Monte Cristo detachment, separating Cenozoic volcanic and sedimentary rocks of the upper plate from underlying Paleozoic-Mesozoic strata and Mesozoic plutons of the lower plate. The Cenozoic rocks constitute two lithologic successions separated by an angular unconformity. The lower sequence is composed of ash-flow tuff, ranging in age from 29-24 Ma, passing upward into rhyolite domes and flows and andesite lava, lahar, and tuff and minor sedimentary rocks, ranging in age from 22 to 17 Ma. The upper Cenozoic sequence is composed of 15 Ma andesite lava, volcaniclastic sedimentary rocks (13 to 11 Ma), and rhyolite (~7 Ma) and basalt flows (7 Ma). Across the region, rocks of the lower Cenozoic sequence exhibit shallow to moderate dips into the basal detachment with all units of the sequence found in direct structural contact with the underlying Paleozoic-Mesozoic basement. The shallowly dipping detachment is characterized by a zone of cataclasite up to one hundred meters thick and is warped in broad northwest-trending folds. The upper Cenozoic section, albeit locally folded and offset by younger high-angle faults, seals the detachment, which was active between 17 and 15 Ma. Displacement on the high-angle faults and detachment system has resulted in the localization and exposure of precious metal deposits in the region.

TABLE OF CONTENTS

LIST OF FIGURES

CHAPTER 1

INTRODUCTION

The northwest-southeast trending transition between the central Great Basin and Sierra Nevada is formed by a belt of late Cenozoic faults that have a complex geometry, history of displacement, and superposition. Active structures within the tectonic belt record transtensional deformation (Oldow, 2003) that initiated between 3 to 5 Ma (Oldow et al., 2008; Walker et al., 2014) and are characterized by coeval transcurrent and extensional faults (Fig. 1). The faults form a mosaic of structural domains characterized by significant differences in geometry and kinematics (Stewart, 1988; Oldow, 1992). In some areas the boundaries between structural domains are gradational but in others transitions are characterized by abrupt juxtaposition of structures with poorly understood kinematic compatibility. The active structures are superposed onto and in many instances reactivate older structures that formed during protracted Miocene to early Pliocene deformation (Stockli et al., 2001; Oldow, 1992; Oldow et al., 2008). The geometry and kinematic history of the older structures is locally obscured by the younger structures and for the most part have only been studied in widely separated parts of the tectonic belt.

The late Cenozoic structures within the deformed belt separating the Sierra Nevada and central Great Basin represent an important element in the tectonic evolution of the North American plate boundary and have contributed to the localization and exposure of substantial mineral resources. The seismically active tectonic belt accommodates about 20 percent of the relative motion between the Pacific and North American plates (Argus and Gordon, 1991; Bennett et al.,

1999; Dixon et al., 2000; Oldow, 2003) and, prior to the onset of contemporary transtensional deformation, was the locus of deformation and volcanism associated with plate-boundary tectonism (Oldow et al., 1989; Burchfiel et al., 1992). The igneous and tectonic history facilitated and localized the deposition of Cenozoic precious metal deposits (John et al., 1989; John, 2001; du Bray et al., 2014; Sillitoe and Lorson, 1994) and displacement on the late Cenozoic structures exhumed and exposed older base-metal and orogenic-gold deposits (Proffett, 1977; Oldow et al, 2003; Craig, 2003). Large tracts of the tectonic belt have not been revisited since earlier geological studies over four decades ago. This lack of study has contributed to significant gaps in the understanding of the structural evolution of this part of the western Great Basin and has inhibited modern mineral exploration in the region. This work included in this thesis is focused on assessing the late Cenozoic structural history of part of this region located in west-central and southwestern Nevada and eastern California (Fig. 1). The results of this work provide constraints needed to better understand the tectonic history of this region and the structural controls on mineral resources. As part of this effort, detailed geologic mapping and structural analysis conducted for this thesis in the northern Silver Peak and Monte Cristo Ranges, the southern Cedar Mountains, and the Royston Hills of west-central Nevada builds on pioneering studies (Ferguson et al., 1953; Robinson and Crowder, 1973; Robinson et al., 1976; Stewart et al., 1994; Whitebread and Hardyman, 1987) and provides insight into the geometry and kinematic history of late Cenozoic high-angle faults and a regionally extensive low-angle detachment system. The high-angle faults form a curved array of structures varying from east-northeast left-oblique faults to north-northwest right-oblique faults that transfer displacement between the northern Eastern California shear zone and southern Walker Lane through the Mina deflection into the central Walker Lane (Fig. 2). Plio-

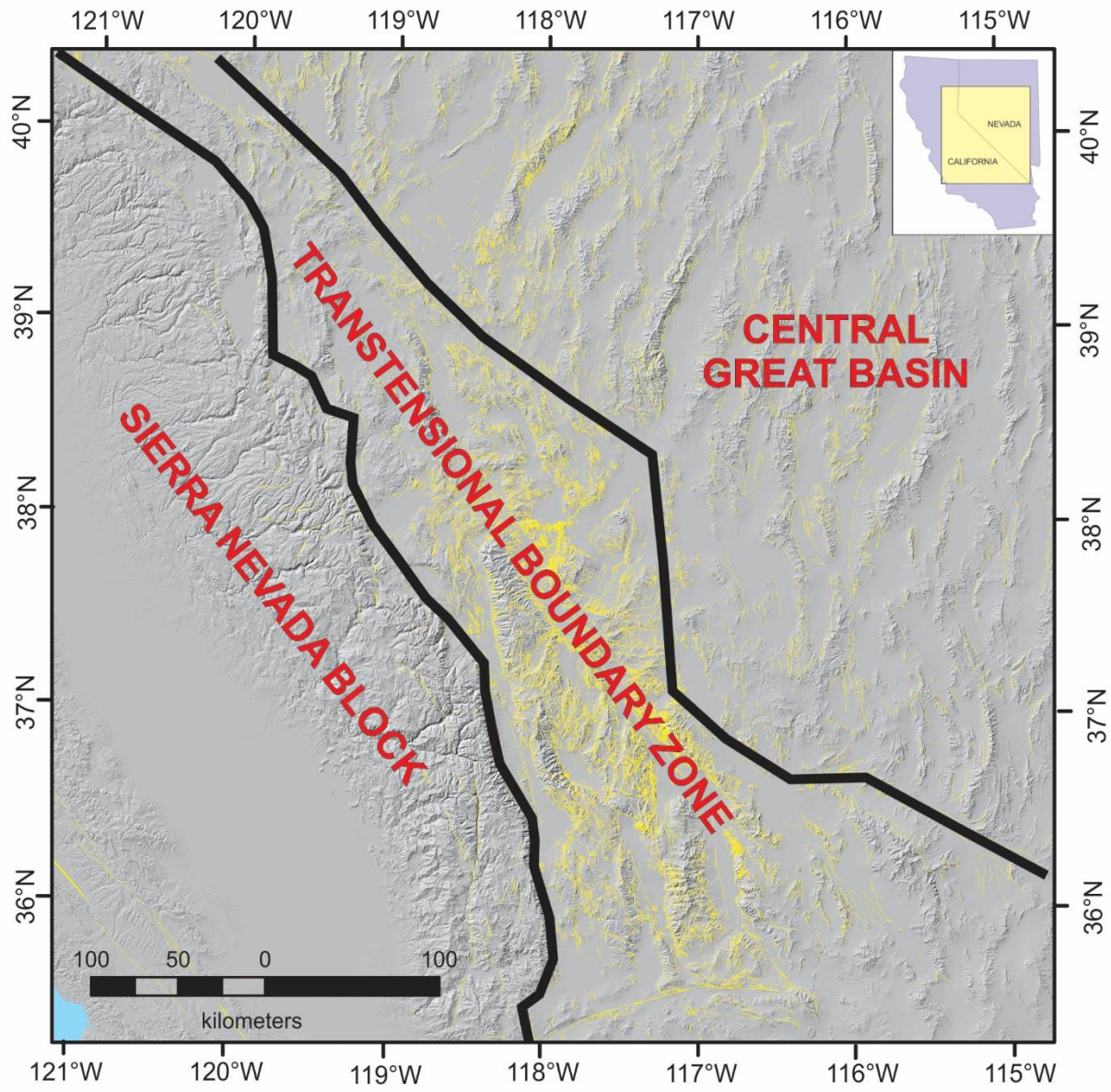

Figure 1. Tectonic domains of the western Great Basin and Sierra Nevada. Yellow lines are Cenozoic high-angle faults. Sierra Nevada block is translating to the northwest at 12-14 mm/yr, away from the east-west extending central Great Basin (based on Global Navigation Satellite System geodesy), resulting in transtensional deformation in the tectonic boundary zone. Inset map in top-right corner shows relative position of study area in California-Nevada.

Pleistocene displacement on these kinematically linked structures is responsible for the dramatic physiographic expression of mountains and basins in the region.

The faults contributed structural controls on precious-metal deposits and to the formation of deep basins that accumulated substantial boron and lithium deposits. Displacement on older Mio-Pliocene high-angle faults and low-angle detachments provided the structural control that localized mineralization in a number of epithermal gold-silver deposits across the region and were also responsible for the exhumation and exposure of Mesozoic base-metal and orogenic-gold systems.

CHAPTER 2

REGIONAL TECTONIC SETTING

The physiographic transition between northeast-trending Basin and Range structure and topography of the central Great Basin and the Sierra Nevada block stretches northwest-southeast for about 780 km (Fig. 1). The broad physiographic boundary is formed by a structural belt of variably oriented transcurrent and extensional faults (Stewart, 1988; Oldow, 1992) that have accommodated between 50 to 100 km of right-lateral displacement and tens of kilometers of extension since the mid-Miocene (Stewart, 1967; Stewart et al., 1988; McKee, 1968; Oldow, 1992, 2003; Snow and Wernicke, 2000). The kinematics and geometry of the structures within this tectonic belt have changed through time. Contemporary transtensional deformation initiated at 3 to 5 Ma (Oldow, 2003; Oldow et al., 2008; Walker et al., 2014) and is accommodated by a complex system of high-angle transcurrent and extensional faults (Stewart, 1988; Oldow, 1992). These faults accommodate the oblique motion resolved onto this boundary zone (Oldow, 2003) and are responsible for the high-relief topography of the region. In contrast, during the mid-Miocene to the Pliocene no significant topographic expression accompanied displacement on high-angle transcurrent and dip-slip dominated faults, which were kinematically linked to low-angle detachment fault systems (Hardyman and Oldow, 1991; Oldow, 1992). The implication is that the older tectonism was not transtensional but rather dominated by wrench mechanisms.

In southeastern California and southwestern Nevada (Fig. 2), the southern part of the tectonic boundary zone is about 130 km wide and 380 km long. Active transtensional fault systems within the belt are structurally heterogeneous and based on significant differences in the

geometry, orientation, and kinematics, are divided into five structural domains (Fig. 2). The region east of the Sierra Nevada, from Owens Valley to Death Valley and Fish Lake Valley (Fig. 3) is bounded by right-lateral to right-oblique fault systems traced laterally for over 250 km. Structures in this region form the northern part of the Eastern California shear zone (Wallace, 1984; Dokka and Travis, 1990), which is bounded by the north-northwest trending Owens Valley – White Mountains fault system to the west and the northwest trending Furnace Creek – Fish Lake Valley fault system to the east. The bounding faults converge to the north and are linked by north-northwest and northeast trending faults initiated at around 4 Ma that relay displacement between the transcurrent structures (Sternlof, 1983; Burchfiel et al., 1987; Reheis and Dixon, 1996). East of the Furnace Creek – Fish Lake Valley fault system, the geometry of structures differ from the area to the west and are assigned to the southern Walker Lane domain (Fig. 2).

Internally, the southern Walker Lane is divided into northern and southern subdomains on the basis of differences in geometry and kinematics of faults. In the south, from southern and central Death Valley eastward to the north-northwest trending boundary with the central Great Basin, the fault pattern is dominated by northeast-striking extensional faults that emanate from the Furnace Creek fault (Fig. 3). The northeast-striking extensional faults transfer displacement eastward to the northwest-striking Stateline fault (Schweickert and Lahren, 1997; Guest et al., 2007; Mahan et al., 2009) and to the north-northwest trending faults along the eastern flank of the boundary zone (Fig. 3). In contrast, the northern segment of the southern Walker Lane, east of northern Death Valley and Fish Lake Valley, is characterized by a system of nearly orthogonal, west-northwest and north-northeast striking faults (Fig. 3). The west-northwest trending faults are left-oblique transcurrent structures (Oldow and Geissman, 2013; Katopody et al., 2016) that are

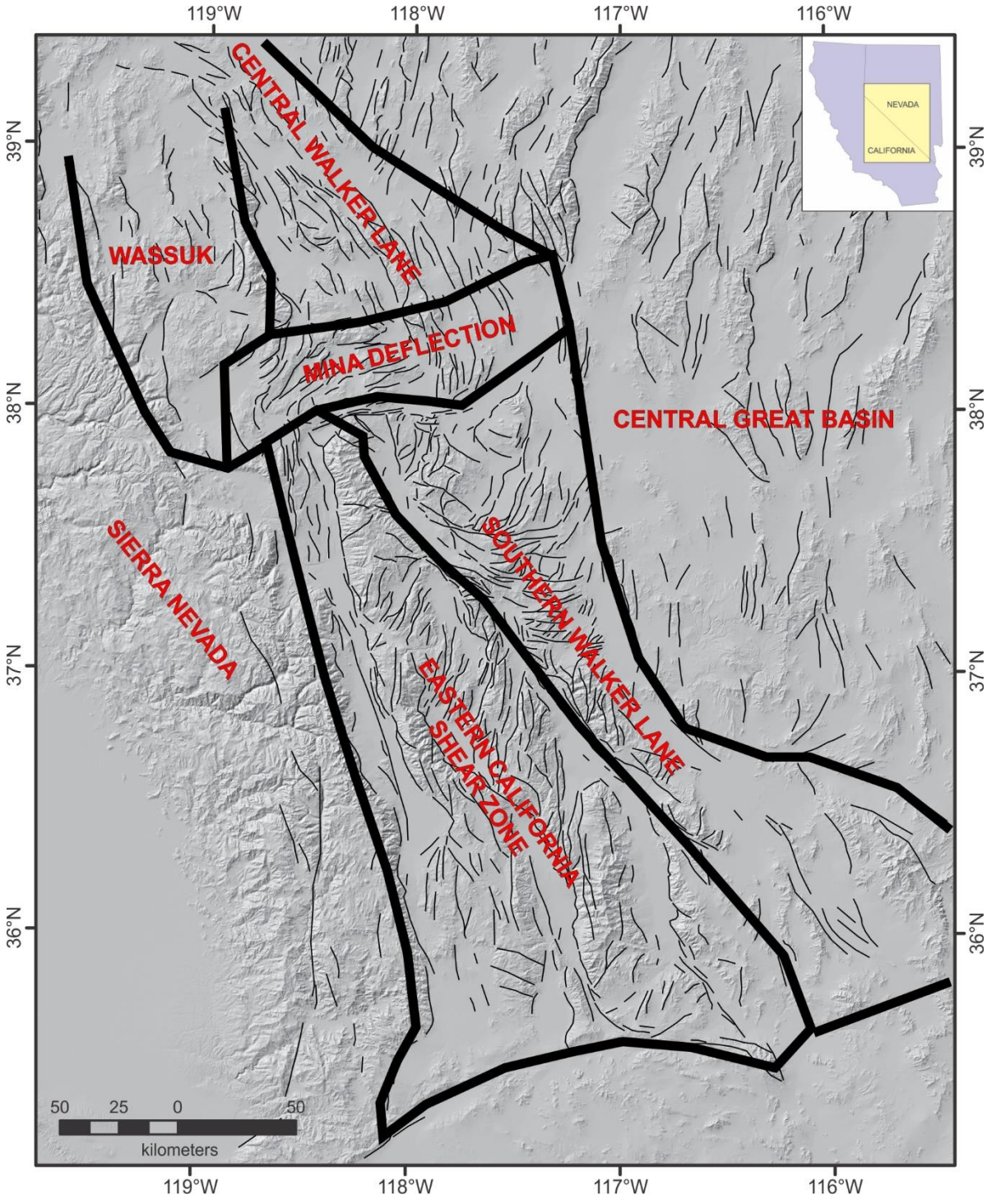

Figure 2. Tectonic domains of the southwestern Great Basin based on the orientations, geometry and kinematics of late Cenozoic high-angle faults.

kinematically linked to north-northeast striking extensional faults. In parts of the region, the extensional faults have trace-lengths of only a few kilometers and transfer displacement between left-oblique structures traced along-strike for 20 to 75 km. In the northern part of the structural domain, the trace-lengths of the extensional faults increases to between 25 to 60 km and these structures transfer displacement to the Mina deflection.

The Mina deflection marks the northern end of the Eastern California shear zone and southern Walker Lane and consists of an east-northeast trending belt of structures about 50 km wide and about 120 km long. Within this belt, east-northeast striking left-oblique and north-northwest striking right-oblique structures are kinematically linked through curved faults that bound deep extensional basins (Oldow, 1992; Oldow et al., 2008; Ferranti et al., 2009). The structures transfer displacement from the northern Eastern California shear zone and southern Walker Lane northward into the central Walker Lane. The central Walker Lane is a narrow (60 km) northwest-trending belt of en echelon, right-lateral transcurrent faults (Ekren et al., 1980; Hardyman and Oldow, 1991; Oldow, 1992) bound to the east by the central Great Basin and to the west by north-northwest striking right-oblique faults of the Wassuk domain, that stretches 75 km west to the Sierra Nevada range front (Fig. 2). Contemporary displacement in the central Walker Lane is characterized by wrench-dominated transtension, whereas in the Wassuk domain displacement is extension-dominated transtension (Oldow, 2003). Older structures, predating the 3-5 Ma onset of transtension, are found in several parts of the tectonic boundary zone. In many areas, the older structures are the antecedents to those currently active, in other areas the older structures were abandoned and cross-cut by younger faults, and in some parts of the region, older structures did not exist or only had minimal displacement.

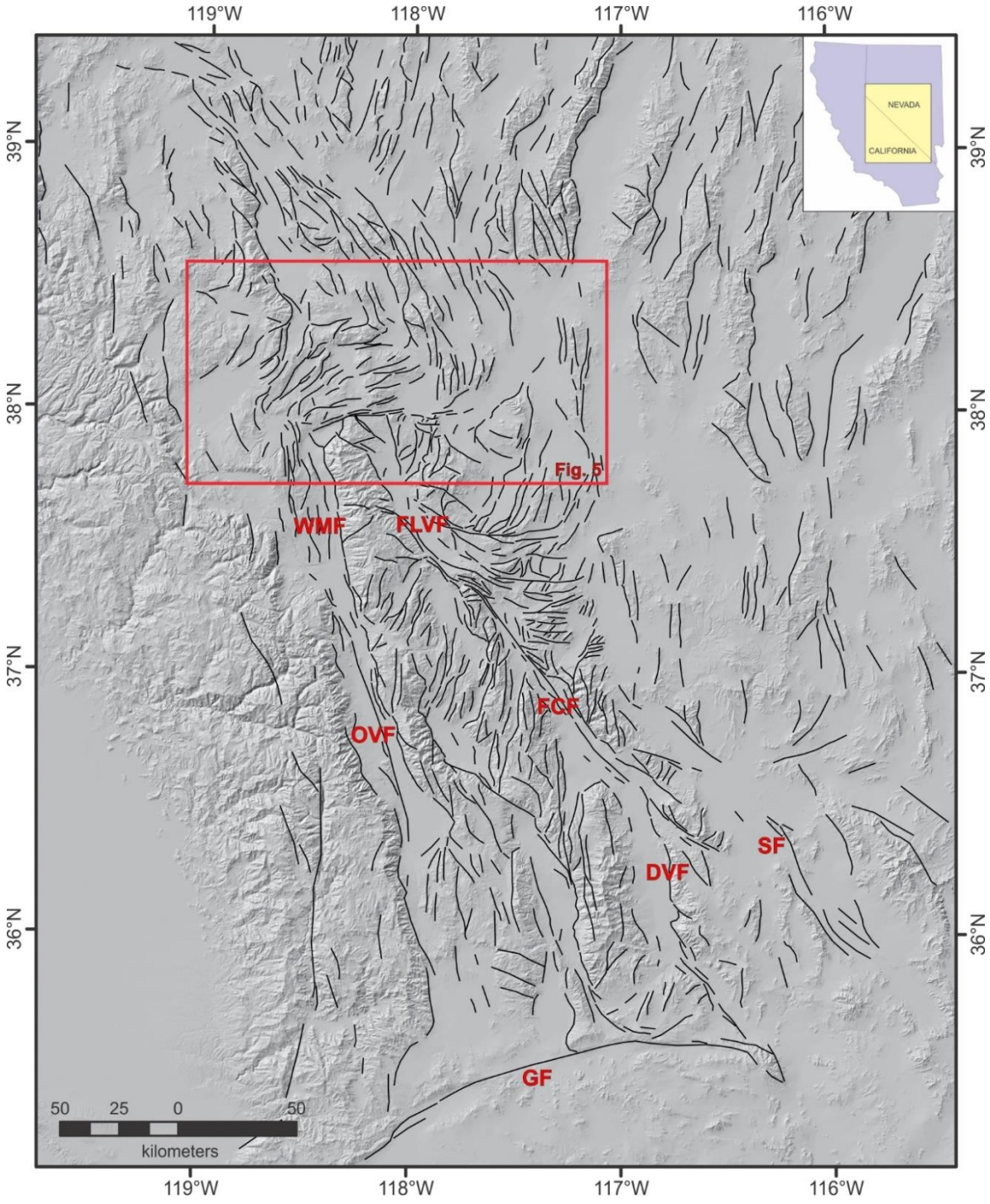

Figure 3. Fault map of the Sierra Nevada and western Great Basin. Extent of Figure 5, the Mina deflection region, is outlined by the red box. Abbreviations: DVF, Death Valley fault; FLVF, Fish Lake Valley fault; FCF, Furnace Creek fault; GF, Garlock fault; OVF, Owens Valley fault; SF, Stateline fault; WMF, White Mountains fault.

In the Eastern California shear zone, older structures with significant displacement appear restricted to areas surrounding and to the west of Death Valley (Fig. 4) and along the Furnace Creek fault system and were superposed on a subdued landscape where mid-Miocene volcanic rocks are traced laterally over tens of kilometers without significant changes in thickness (Niemi et al., 2001; Walker et al. 2014). Detachment faults responsible for 80 to 135 km of northwesterly extension (Stewart, 1983; Wernicke et al., 1988; Serpa and Pavlis, 1996) are recognized in an east-west trending belt from the Black Mountains west to the Slate Range (Fig. 4) in southeastern California. In the Black Mountains and Panamint Range, detachment faults exhumed mid-crustal metamorphic tectonites in their lower plates and in the Slate Range exposed plutonic rocks and metasedimentary and metavolcanic rocks. The structures were active since the mid-Miocene (Hodges et al., 1990; Holm and Wernicke, 1990; Miller and Pavlis, 2005; Walker et al., 2014; Bidgoli et al., 2015) and may be dismembered segments of a single regionally extensive structure disarticulated by younger transtensional faults (Walker et al., 2014).

Further north in the Eastern California shear zone, little evidence supports large magnitude deformation prior to the Pliocene opening of Owens Valley (Bachman, 1978) and Fish Lake Valley (Reheis and Sawyer, 1997). Zircon and apatite fission-track cooling histories from plutonic rocks in the White and Inyo Mountains (Stockli et al., 2003; Lee et al., 2009) are interpreted to indicate periods of extension and tilting at about 12 and 16 Ma, respectively, but the degree of exhumation and the magnitude of displacement on faults active during this time appears to be relatively modest. Easterly tilts of about 15° and 25° of the southern and northern parts of the White Mountains (Fig. 4), respectively, are recognized from the attitude of sedimentary and volcanic rocks resting on Mesozoic plutons and metasedimentary rocks (Reheis and Sawyer, 1997; Lueddecke et al., 1998;

Stockli et al.,2003). Although attributed to a period of rapid exhumation and tilting at about 12 Ma (Stockli et al., 2003), this interpretation is difficult to reconcile with geologic observations. In the southern White Mountains, the 15° easterly tilt of the mountain range postdates deposition of areally extensive basalt flows dated by $^{40}Ar/^{39}Ar$ as 6.06 Ma (Oldow, unpublished data). Similarly, easterly tilts in the northern part of the range, expressed by the attitudes of Miocene to Pliocene rocks, indicate little easterly tilt had occurred before the Pliocene. Sedimentary and volcanic rocks dated by K-Ar as 11.5 ± 0.4 Ma dip east at 25°, and are overlain unconformably by volcanic rocks dated at 3 to 4 Ma using K-Ar (Reheis and Sawyer, 1997; Stockli et al., 2003). The Pliocene volcanic rocks typically dip east 15° to 20°, allowing only 5 to 10 degrees of easterly tilt to be attributable to pre-Pliocene extension. In the Inyo Mountains, a period of cooling at about 16 Ma is explained by exhumation and westerly tilting of the mountain range (Lee et al., 2009). Where the thermochronology study was conducted, there are no Cenozoic rocks exposed in the range to substantiate this interpretation, but 30 km farther south, Miocene conglomerate and sandstone containing a reworked tuff horizon dated by $^{40}Ar/^{39}Ar$ at 13.6 ± 0.5 Ma (Conrad, 1993) are essentially flat-lying. The Miocene clastic rocks reach a thickness of about 350 m and are interpreted (Conrad, 1993) to record a period of extensional faulting that may be associated with the cooling history identified farther north. The clastic rocks are bound on the east and west by active extensional faults removing any reliable estimate of the throw on faults thought to exist during deposition. Nevertheless, based on the lateral extent of late Miocene to Pliocene basalt across the region, very modest topographic relief is indicated before the onset of transtensional deformation (Burchfiel et al., 1987, Sternlof, 1983).

The northern part of the Furnace Creek – Fish Lake Valley fault was clearly active during the mid-Miocene to Pliocene and accommodated about 20 km of a total of 45-50 km of right lateral displacement, constrained in this area by the offsets of Jurassic plutonic rocks (McKee, 1968; Reheis and Sawyer, 1997; Mueller et al., 2016a; Mueller and Oldow, 2017). During this early stage of movement, the right-lateral displacement on the Furnace Creek – Fish Lake Valley (FCFLV) fault system was transferred to the central Walker Lane via the shallowly northwest-dipping detachment fault of the Silver Peak – Lone Mountain (SPLM) extensional complex (Oldow et al., 1994, 2009). Northwest-directed transport of the upper-plate of the SPLM complex resulted in localized synextensional deposition of late Miocene to early Pliocene sedimentary and volcanic rocks (Oldow et al., 2009) as metamorphic tectonites were exhumed in the lower plate exposed in the central Silver Peak Range, Weepah Hills, and Lone Mountain (Fig. 4). The SPLM detachment system was active from 11 to 5 Ma, based on fission-track and (U-Th)/He cooling ages from the underlying basement rocks and radiometric ages of the overlying synextensional volcanic and sedimentary rocks (Oldow et al., 1994, 2008). The detachment and associated upper-plate faults were cross-cut by younger high-angle structures formed after the onset of transtension at about 3 to 5 Ma (Oldow et al., 2008).

Prior to initiation of displacement on the FCFLV fault system and the SPLM detachment, east-west trending half-grabens formed in parts of the region and accumulated up to 2.0 km of early Miocene andesite flows and lahar and sedimentary rocks (Kerstetter et al., 2016a). The displacement and accumulation of rocks in half-grabens across the region was active during the late Oligocene and early Miocene and ceased before being overlapped by mid-Miocene andesite (15 Ma) and ash-flow tuff (Kerstetter et al., 2016a, 2016b). Two half-grabens are well preserved

along the southern flank of the SPLM complex and are between 10-15 km long and 5-10 km wide. The half-grabens are offset from one another by at least 10 km and structurally linked by north-south trending faults forming a dog-leg pattern of east-west and north-south faults. Elsewhere in this region, the existence of late Oligocene to early Miocene half-grabens is inferred on the basis of major stratigraphic thickness variations across high-angle faults, but the basins are highly fragmented by younger structures.

Many aspects of the history of older structures in the southern Walker Lane south of the SPLM complex remain obscure. Much of the structural domain is concealed beneath alluvial deposits of Sarcobatus Flat and the Amargosa Desert (Fig. 4). Exposures of pre-Cenozoic bedrock and Cenozoic volcanic rocks are found in the ranges between and to the west of these basins (Bullfrog Hills, Funeral, Grapevine and Gold Mountains, and Slate Ridge), but access to these areas is extremely limited and geologic mapping sparse. Nevertheless, detailed work in parts of the region (Maldonado, 1990), together with unpublished mapping (Oldow and Katopody, personal communication) indicates that the mountains expose a regionally extensive system of low-angle detachment faults that were active during the Miocene. Detachment faults were active in the Bullfrog Hills from about 13 to 8 Ma (Hoisch et al., 1997) where amphibolite-facies metamorphic basement was exhumed as upper-plate tuff and Paleozoic layered rocks were tilted (Maldonado, 1990). Similarly, in the Funeral Mountains, exhumation of amphibolite-facies basement rocks by a detachment fault which was active from about 11 to 6 Ma (Holm and Dokka, 1991; Hoisch and Simpson, 1993) and subsequently crosscut by younger range-front faults (Bidgoli et al., 2015). Detachment faults separating tilted Miocene ash-flow tuff and pre-Cenozoic layered rocks above a lower-greenschist basement complex is recognized in the northern

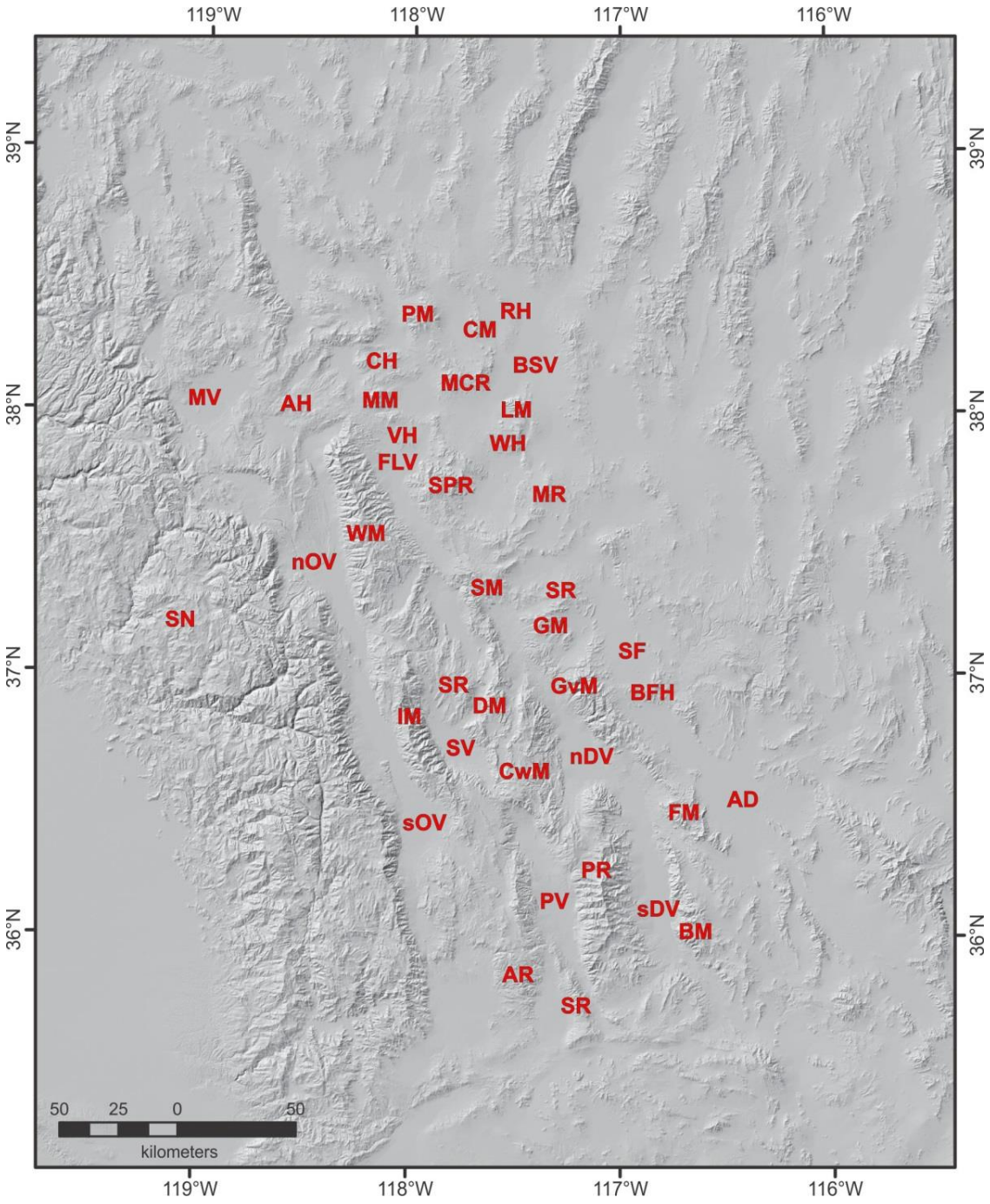

Figure 4. Geographic areas referenced in text. Abbreviations: AH, Adobe Hills; AR, Argos Range; AD, Amargosa Desert; BSV, Big Smoky Valley; BM, Black Mountains; BFH, Bullfrog Hills; CH, Candelaria Hills; CM, Cedar Mountains; CwM, Cottonwood Mountains; DM, Dry Mountains; FLV, Fish Lake Valley; FM, Funeral Mountains; GM, Gold Mountain; GvM, Grapevine Mountains;

(Fig. 4 continued): IM, Inyo Mountains; LM, Lone Mountain; MM, Miller Mountain; MV, Mono Valley; MCR, Monte Cristo Range; MR, Montezuma Range; nOV, northern Owens Valley; sOV, southern Owens Valley; PR, Panamint Range; PM, Pilot Mountains; RH, Royston Hills; SR, Saline Range; SV, Saline Valley; SF, Sarcobatus Flat; SPR, Silver Peak Range; SR, Slate Range; SN, Sierra Nevada; SM, Sylvania Mountains; VH, Volcanic Hills; WH, Weepah Hills; WM, White Mountains.

Grapevine Mountains, Gold Mountain and Slate Ridge region (Fig. 4). Based on the age of tilted Miocene tuff and overlapping volcanic rocks, activity on this detachment system occurred between 14 and 8 Ma (Oldow, unpublished mapping; Worthington, 1992; Niemi, 2012). In addition to detachment faults, the southern and central segments of the Furnace Creek fault were active with an inception of right-lateral motion at 12 to 8 Ma (Stewart, 1966; Serpa and Pavlis, 1996). Based on timing constraints, the Furnace Creek fault and the detachment faults were active contemporaneously, but their tectonic arrangement remains as a source of controversy (Burchfiel and Stewart, 1966; Stewart, 1967; Serpa and Pavlis, 1996). The incomplete knowledge of the role of strike-slip deformation in the region is exemplified by the uncertainty in possible kinematic linkage of the Furnace Creek fault and the northwest-striking Stateline fault (Fig. 3) 16 km east in the Amargosa Desert region (Schweickert and Lahren, 1997; Guest, 2017; Mahan et al., 2009). The Stateline fault accommodates 25 to 30 km of right-lateral displacement since 13 Ma, but questions remain about possible displacement transfer between the Stateline and Furnace Creek faults and when motion initiated on the Stateline fault (Guest et al., 2007).

In the area north of the Mina deflection, Oligocene to Pliocene deformation differs substantially in timing and kinematics across the region. In the central Walker Lane, long trace-length transcurrent faults were active as early as 25 Ma (Hardyman and Oldow, 1991) and formed together with east-west trending half-grabens and detachment faults (Ekren et al., 1980; Hardyman

and Oldow, 1991; Oldow, 1992). Several east-west trending half-grabens, ranging from 10-15 km long and 5-10 km wide, localized 1.0 to 1.5 km thick accumulations of Oligocene ash-flow tuff and Miocene andesite (Hardyman and Oldow, 1991; Kerstetter et al., 2016b). The half-grabens were linked by north to northwest striking transcurrent faults in a geometry similar to that of the well exposed structures in the southern Walker Lane (Kerstetter et al., 2016a, 2016b). Unlike the half-grabens, which formed as isolated structures throughout the central Walker Lane, detachment faults are more spatially restricted and found in proximity to major transcurrent faults (Ekren et al., 1980; Hardyman and Oldow, 1991). The detachment faults cut volcanic rocks ranging in age from 25 to 22 Ma but are not found in younger successions. The 25-22 Ma volcanic rocks are locally tilted up to 70° by listric normal faults that do not penetrate into the underlying basement but which rather sole into the detachment faults separating the Cenozoic cover and pre-Cenozoic rocks. The detachment faults formed at low angle and are kinematically linked to steeply dipping transcurrent faults (Hardyman and Oldow, 1991). The timing relations between displacement on the transcurrent faults, east-west trending half-grabens, and detachment faults suggest a related origin, possibly with detachment fault formation occurring late during a limited time in the deformation history. Activity on detachment faults and half-grabens ceased prior to deposition of 19-15 Ma andesite (John, 1992; Garside, 1979; Kerstetter et al., 2016b), possibly at different times in different areas. Farther to the west, in the Wassuk domain (Fig. 2), large-scale crustal extension dated between 14 and 11 Ma was accommodated by the progressive tilt of fault blocks (Proffett, 1977; Dilles and Gans, 1995). Although now at a low-angle, the normal faults are not detachment structures like those observed in the central Walker Lane and formed as listric normal faults that penetrated deep into the crust. Displacement on successive generations of structures resulted in

profound crustal tilting (Proffett, 1977; Proffett and Dilles, 1984; Dilles and Gans, 1995). For decades, the incomplete understanding of the late Cenozoic history of deformation within the Mina deflection has presented a significant obstacle in relating the structural histories of the west-central Nevada and region to the south in southwest Nevada and eastern California. As outlined in the sections below, there are similarities in the history of older Cenozoic structures throughout the region, but also significant differences that remain unresolved.

CHAPTER 3

GEOLOGY OF THE MINA DEFLECTION

3.1 Introduction

The Mina deflection was originally identified on the basis of an offset or step in the earthquake epicenters of west-central Nevada (Ryall and Priestly, 1975). Over the years, the designation has expanded, and the region is now recognized as an east-northeast trending belt of high-angle faults linking coeval structures in the northern Eastern California shear zone, the southern Walker Lane, and central Walker Lane (Stewart, 1988; Oldow, 1992, 2003). The tectonic belt stretches from northern Owens Valley in California east for about 120 km to Big Smoky Valley in Nevada (Fig. 4). In the western half of the structural domain, a north-south extent of about 50 km is clearly defined by bounding east-northeast striking transcurrent faults. To the east, the southern boundary is well marked by northeast-striking faults but to the north, faults progressively change orientation from northeast to north-northwest (Fig. 5) making the boundary between the eastern Mina deflection and southern central Walker Lane arbitrary in nature.

3.2 Lithology of the Mina deflection region

The Mina deflection region is underlain by thick successions of Proterozoic and Mesozoic layered rocks and Mesozoic plutons. The rocks straddle the curvilinear trace of the late Precambrian edge of continental North America, which is demarcated by the initial strontium 0.706 isopleth determined from Mesozoic plutons scattered across the region (Kistler

and Peterman, 1978; Kistler, 1978; Saleeby, 1986; Elison et al., 1990). The ancient continental boundary juxtaposes continental and non-continental crust over a distance of about 50 km and has contributed to the complex and spatially variable pre-Cenozoic stratigraphy found in this region. Along the southern margin of the Mina deflection, the stratigraphic succession is composed of over 15 km of Proterozoic and Paleozoic carbonate and siliciclastic rocks that were deposited in the North American miogeosyncline (Oldow et al., 1989; Burchfiel et al., 1992). In contrast, Triassic to Jurassic carbonate, siliciclastic, and volcanic rocks of the Mesozoic marine province (Speed, 1978; Oldow, 1984; Oldow et al., 1993) to the north were accumulated in a back-arc basin underlain by non-continental crust (Oldow, 1983; Oldow et al., 1989; Burchfiel et al., 1992). Within the intervening region underlying the Mina deflection, late Paleozoic clastic and carbonate rocks are locally overlain by Mesozoic layered rocks and all are intruded by Jurassic to Cretaceous plutons (Ross, 1961; Albers and Stewart, 1972). The Phanerozoic layered rocks of this part of the western Great Basin are cut by and locally overlap a complex system of Paleozoic and Mesozoic thrusts. The Precambrian crustal boundary controlled the locus of successive contractional tectonism (Oldow et al.,1989; Burchfiel et al., 1992) recorded by the east-west trending segments of the mid-Paleozoic Roberts Mountains thrust (Oldow, 1984), the late Paleozoic to early Mesozoic Golconda thrust (Speed, 1977, 1979) and the Mesozoic Luning-Fencemaker thrust (Oldow, 1981, 1983, 1984, 1992). The pre-Cenozoic basement succession is overlain by several kilometers of volcanic and volcaniclastic sedimentary rocks of Oligocene to Quaternary age.

The Cenozoic stratigraphy is characterized by significant lateral variations in composition, spatial distribution, and thickness across the region. In general, the succession is

divided into a lower and upper sequence separated by a regionally extensive angular unconformity formed in the mid-Miocene. The lower part of the Cenozoic sequence consists of Oligocene ash-flow tuffs that typically rest on pre-Cenozoic basement, but which locally are separated from the basement by relatively thin andesite flows and lahar deposits. Where found, the Oligocene andesite succession is typically several tens of meters thick and has often experienced extensive hydrothermal alteration. Oligocene rhyolitic ash-flow tuff consists of several assemblages that were derived from three distinct source areas; the tuff units from individual source areas can be traced laterally for up to 130 km but are not interleaved. The boundaries between the widespread tuff assemblages are abrupt, suggesting broad regions with modest topography separated by relatively narrow areas with sufficient relief to restrict passage of the ash-flow tuffs. Within the regions of modest topographic relief, cooling unit thicknesses are typically several tens of meters but generally less than 100 m. In areas where accommodation space was controlled by active half-graben basins, however, individual cooling units can reach up to 200 to 250 m thick and the ignimbrite succession as a whole increases to 1.5 km (Speed and Cogbill, 1979; Hardyman and Oldow, 1991; Kerstetter et al., 2016a, 2016b; Kerstetter and Oldow, 2016). The Oligocene tuff succession is overlain by a sequence of andesite lahar, tuff, flows, and minor sedimentary rocks with thicknesses ranging from a few hundred meters to 1.5 km thick. The thick accumulations are spatially restricted to the axes of east-west trending synextensional half-grabens that are typically 2-5 km wide and 5-10 km long (Hardyman and Oldow, 1991; Kerstetter et al., 2016a. 2016b). The andesite succession locally passes upward into several hundreds of meters of volcaniclastic rocks that appear to have a spatially restricted distribution across the region (Stewart et al., 1994).

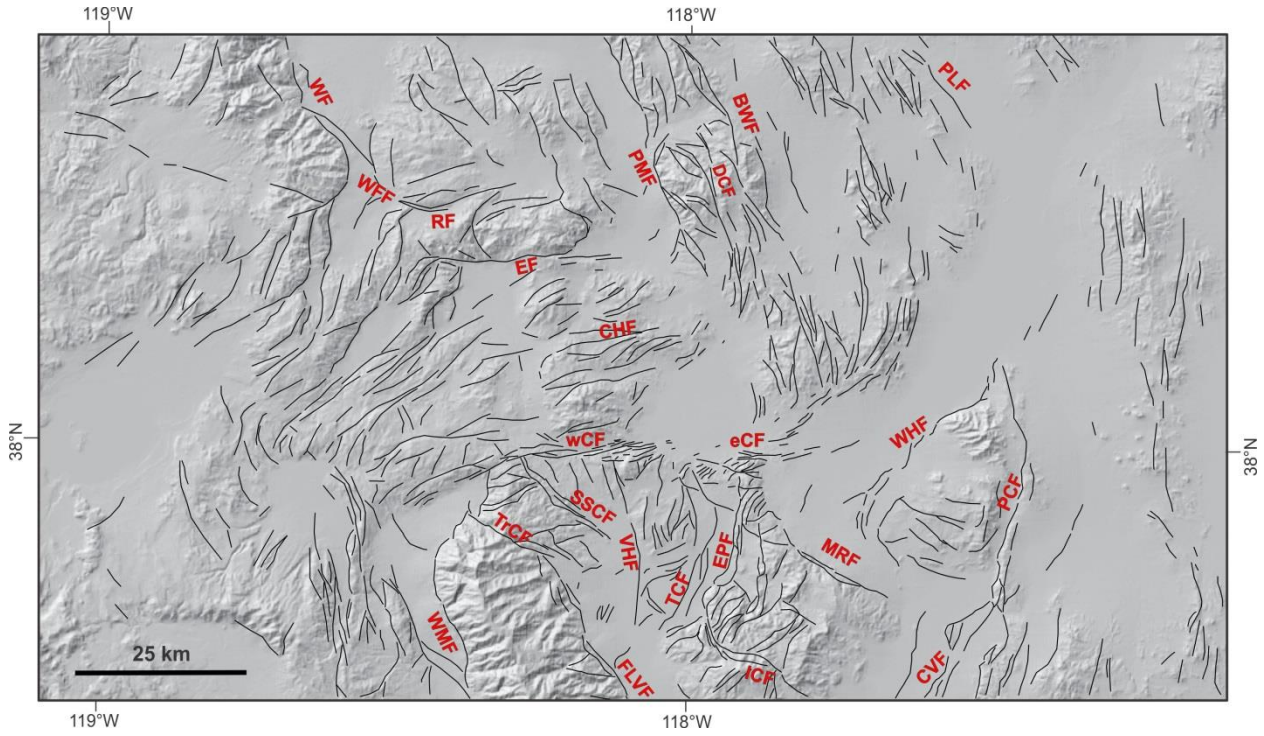

Figure 5. Fault map of the Mina deflection region. Abbreviations: BWF, Bettles Well fault; CHF, Candelaria Hills fault; CLV, Clayton Valley fault; eCF, eastern Coaldale fault; wCF, western Coaldale fault; DCF, Dunlap Canyon fault; EPF, Emigrant Peak fault; EF, Excelsior fault; FLVF, Fish Lake Valley fault; ICF, Icehouse Canyon fault; PCF, Paymaster Canyon fault; PMF, Pilot Mountain fault; PLF, Pole Line fault; RF, Rattlesnake fault; SSCF, Sand Springs Canyon fault; TCF, The Crossing fault; TrCF, Trail Canyon Fault; VHF, Volcanic Hills fault; WHF, Weepah Hills fault; WF, Wassuk fault; WFF, Whisky Flat fault; WMF, White Mountain fault.

The upper sequence of Cenozoic rocks is composed of Miocene andesite flows and lahar deposits with a relatively constant thickness of 60 to 100 m across the region. The andesite flows and lahar deposits are overlain conformably by Miocene volcaniclastic fluvial and lacustrine sedimentary rocks. The sedimentary rocks contain tuff interbeds and range in

thickness from a few hundred meters to at least 2.5 km (Robinson et al., 1976 Stewart and Diamond, 1990; Diamond and Ingersoll, 2002; Oldow et al., 2009). The sedimentary succession is variously overlain by late Miocene rhyolite and latite ash-flow tuff, rhyolite flows and domes, and basalt. The rhyolite and latite ash-flow tuff units are localized within upper-plate synextensional basins of the SPLM extensional complex (Oldow et al., 1994, 2009), whereas the rhyolite flows and domes are found outside of the SPLM but have limited spatial extent (Stewart et al., 1994). Basalt is widespread across the region and ranges from mid-Miocene to Quaternary age. Basalt of mid-Miocene age (11.5 Ma) typically is on the order of meters to tens of meters thick and widespread across the region south of the Mina deflection (Mueller and Oldow, 2017), suggesting little topographic relief during deposition. Younger basalt, (7 to 3 Ma) is widespread and locally interleaved with Plio-Pleistocene volcaniclastic fluvial and lacustrine sedimentary rocks (Reheis, 1991). The sedimentary rocks and basalt typically are spatially isolated in different parts of the region, with basalt being more prevalent in the north and west. The Plio-Pleistocene sedimentary succession is exposed within and along the flanks of several mountain ranges and passes upward into overlying contemporary basin-fill deposits.

3.3 Structure of the Mina deflection region

The southern and northern boundaries of the western Mina deflection are marked by the east-northeast striking high-angle faults (Fig. 5) of the Coaldale fault system and Excelsior fault system, respectively (Stewart, 1988). The western part of the tectonic belt is characterized by a distributed array of east-northeast faults that are traced along-strike for distances up to 35 km. The east-northeast faults transition from the north-northwest faults of the Owens Valley region in

eastern California through a curved array of structures (Oldow, 1992; Nagorsen-Rinke et al., 2013). The east-northeast trending faults emerge from the curved fault array as closely spaced, anastomosing splays with strand separation ranging from hundreds of meters to 5 km. In areas where spacing is on the order of a few kilometers, the east-northeast trending faults are often linked by northerly trending structures. Along the northern boundary, north-northeast faults emanate from the east-northeast fault array and change strike orientation into alignment with northwest trending structures of the central Walker Lane (Fig. 5).

In the central and eastern parts of the Mina deflection the structural pattern changes from what is observed in the west. The southern boundary of the central Mina deflection, marked by the Coaldale fault zone, is impinged upon at high-angles by a horsetail array of faults forming the northern terminus of the Furnace Creek – Fish Lake Valley fault system (Fig. 5). From west to east over a distance of about 45 km, the horsetail faults strike from northwest through north-south to north-northeast and abruptly terminate into the east-northeast trending Coaldale fault zone. Farther to the east, the southern margin of the structural domain is diffuse and the Coaldale fault zone loses definition east of the Silver Peak Range as it enters Big Smoky Valley, and the boundary with the southern Walker Lane is formed by northeast-striking faults along the northern Weepah Hills and Lone Mountain (Figs. 5 and 6). Within the central part of the Mina deflection, the western belt of east-northeast faults curve around deep extensional basins, such as Rhodes and Columbus Salt Marshes, and emerge as north-northwest faults that extend northward into the central Walker Lane. At the apex of the curved fault arrays, displacement is dip-slip dominated and localizes the formation of pull-apart basins with depths, determined by inversion of gravity data, of up to 3 to 4 km (Oldow, 1992; Ferranti et al., 2009). The curved faults transfer the left

-

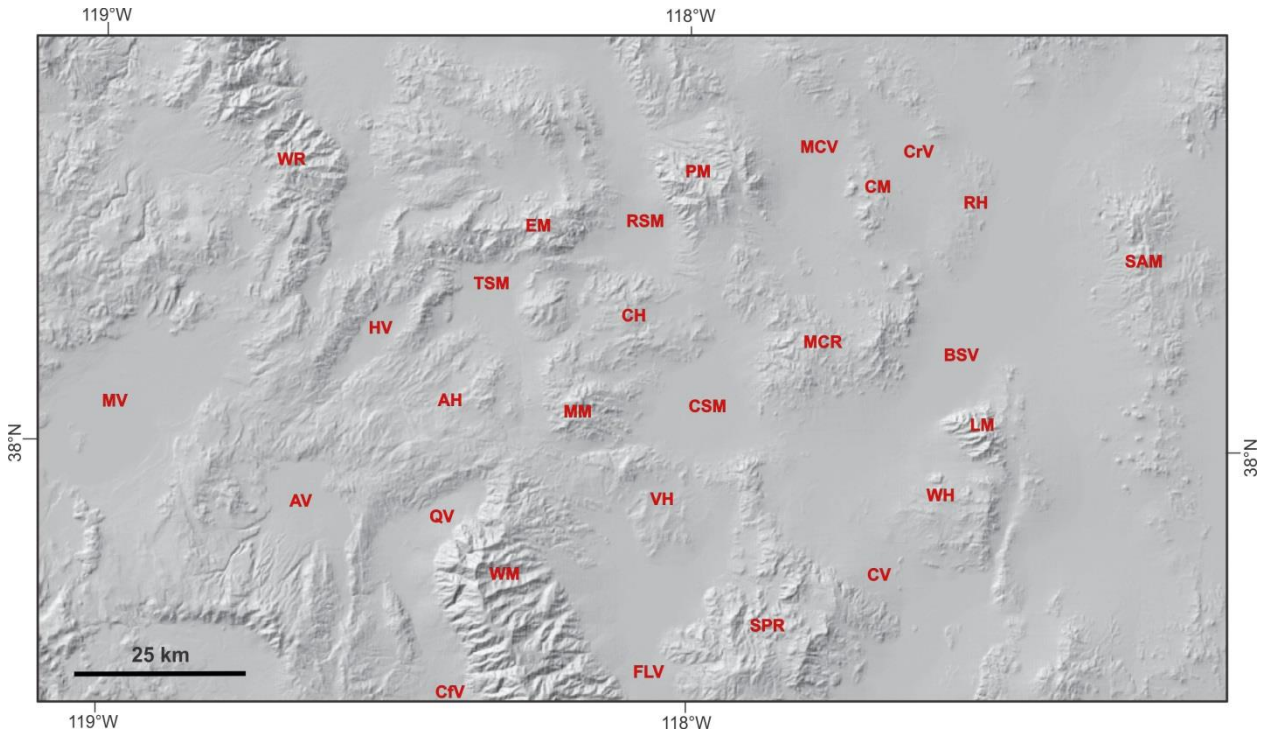

Figure 6. Geographic areas referenced in text. Abbreviations: AV, Adobe Valley; AH, Adobe Hills; BSV, Big Smoky Valley, CM, Cedar Mountains; CfV, Chalfant Valley; CrV, Cirac Valley; CV, Clayton Valley; CSM, Columbus Salt Marsh; EM, Excelsior Mountains; FLV, Fish Lake Valley; HV, Huntoon Valley; LM, Lone Mountain; MM, Miller Mountain; MV, Mono Valley; MCR, Monte Cristo Range; MCV, Monte Cristo Valley; PM, Pilot Mountains; QV, Queen Valley; RH, RSM, Rhodes Salt Marsh; Royston Hills; SAM, San Antonio Mountains; SPR, Silver Peak Range; TSM, Teels Salt Marsh; VH, Volcanic Hills; WR, Wassuk Range; WH, Weepah Hills; WM, White Mountains.

oblique displacement of the east-northeast structures to right-oblique displacement on north-northwest faults.

Active high-angle faults are superposed onto older east-west trending half-grabens and a system of low-angle detachment faults. The eastern part of the Mina deflection exposes a

regionally extensive detachment fault system, named here the Monte Cristo detachment, which separates Oligocene to mid-Miocene volcanic and sedimentary rocks in the upper-plate from underlying Paleozoic and Mesozoic sedimentary and Mesozoic plutonic rocks in the lower-plate. Although recognized in the Royston Hills thirty years ago by Whitebread and Hardyman (1988), the detachment is only now recognized as a regionally extensive feature (Cland and Oldow, 2017) that is exposed over a region of about 1,800 km^2. The detachment underlies a region stretching from the south-central Mina deflection southeast to the boundary with the central Great Basin and thence northwest for about 45 km (Fig. 7). The Monte Cristo detachment formed with a shallow dip as demonstrated by the lack of tilt of folds and thrusts in the underlying basement rocks. Importantly, the detachment was not formed by large-scale crustal tilting like that observed in the Yerington district 150 km to the northwest (Proffett, 1977) and proposed for the Hall district along the eastern boundary of the Mina deflection (Shaver and McWilliams, 1987). The upper- and lower-plates of the Monte Cristo detachment are deformed in folds with amplitudes of several hundreds of meters and half-wavelengths of 5 to 10 km. The folded detachment and rocks of the upper and lower plates are unconformably overlain by mid-Miocene to Quaternary volcanic and sedimentary rocks. Based on the ages of the youngest rocks involved in detachment structures and the oldest unconformably overlying rocks, activity on the structure is restricted to between about 17 and 15 Ma (Cland and Oldow, 2017).

In light of the prevalence of detachment structures throughout this region, it is important to understand how the Monte Cristo detachment relates to the low-angle structures exposed to the north and south, in the central and southern Walker Lane, respectively. The Monte Cristo detachment is distinct and separate from the low-angle faults formed in the SPLM extensional

complex to the south. The structures in the SPLM complex are younger than the Monte Cristo detachment and exhume deep crustal rocks in their footwall. Unlike the Monte Cristo detachment, the upper-plate of the SPLM complex contains both Cenozoic volcanic and sedimentary rocks, Mesozoic plutons, and weakly metamorphosed Paleozoic rocks. The relationship between the Monte Cristo detachment and low-angle faults in the central Walker Lane, on the other hand, is not established. The detachment faults in both regions formed with shallow dips and separate tilted Cenozoic volcanic and sedimentary rocks from underlying pre-Cenozoic basement rocks. The detachments have spatially restricted distributions with known or possible association with long trace-length transcurrent faults and are cross-cut and offset by belts of active transcurrent structures. The Monte Cristo detachment appears to be younger than the detachment faults farther north, but a single age of structural development is not established in the central Walker Lane (Hardyman and Oldow, 1991).

Although widespread, the Monte Cristo detachment is not found in the western and central parts of the Mina deflection. To the north and west of Columbus Salt Marsh (Fig. 6) in Miller Mountain, the Candelaria Hills and the Adobe Hills, and north in the southern Pilot Mountains, no evidence supports the existence of low-angle detachment faults and Oligocene tuff rests depositionally on Paleozoic rocks. In these areas, where structural and stratigraphic relations are well preserved, late Oligocene tuff and early Miocene andesite are observed to achieve thicknesses of over 1.5 km within east-west trending half grabens and to exhibit the prismatic stratal patterns indicative of synextensional deposition (Speed and Cogbill, 19779 Kerstetter et al., 2016b). All of the rocks within the Mina deflection have experienced clockwise, vertical-axis rotation between 20° to 30°, and paleomagnetic investigation of Cenozoic volcanic rocks ranging from Oligocene

to early Pliocene age all see comparable rotations (Petronis et al., 2002, 2009). The rotation of volcanic rocks is observed throughout the domain and is, on this basis, not related to displacement on observed detachment faults. Rather, the rotation appears to be associated with large-scale distributed deformation that may predate the onset of the contemporary transtensional deformation (Oldow et al., 2008) but may be ongoing.

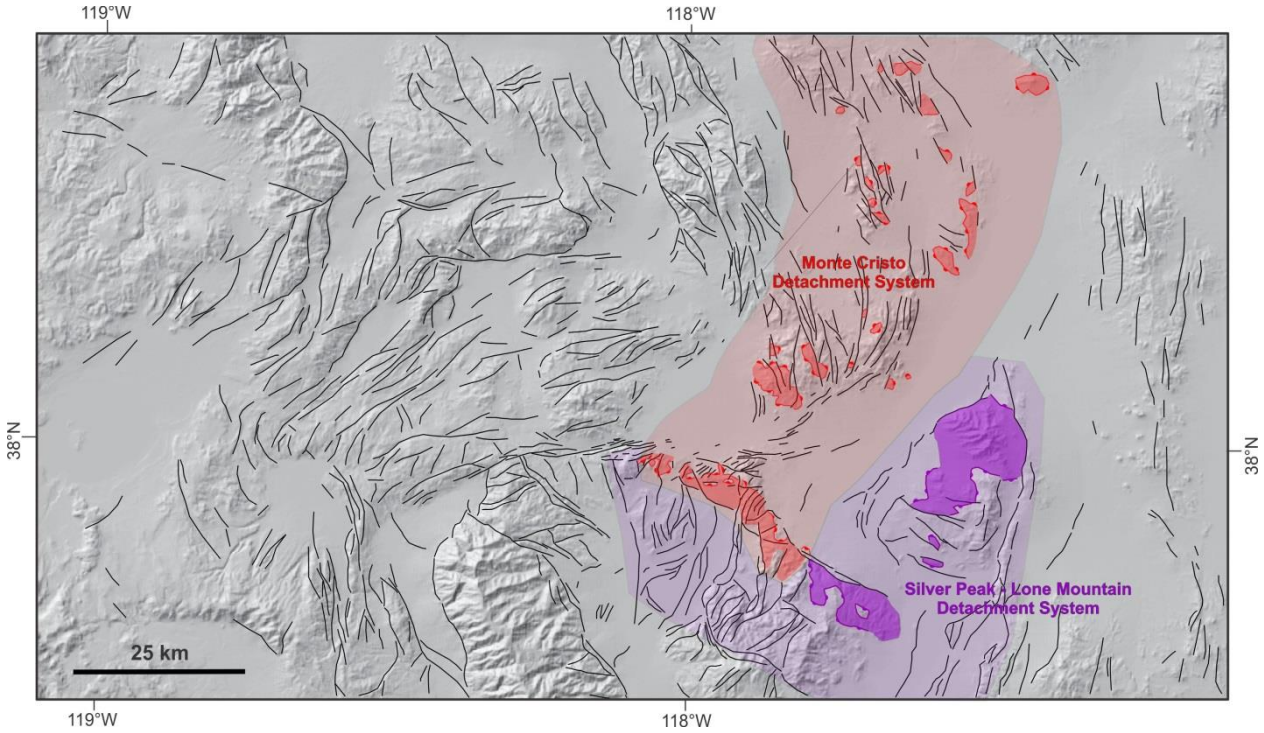

Figure 7. Fault map showing high-angle faults of the transtensional tectonic regime superposed onto older low-angle detachment faults. Red, low-angle faults of the Monte Cristo detachment system, teeth on upper plate; red fill region underlain by structures. Purple, low-angle faults of the Silver Peak – Lone Mountain extensional complex, teeth on upper plate, purple fill region underlain by structures.

CHAPTER 4

GEOLOGY OF THE NORTHERN SILVER PEAK RANGE AND VOLCANIC HILLS

4.1 Introduction

The morphology of the northern Silver Peak Range and Volcanic Hills reflects the orientation of the nearly orthogonal fault systems juxtaposed along the boundary between the Mina deflection and southern Walker Lane. The mountains make a right-angle bend with an east-west trending segment separating northern Fish Lake Valley and Columbus Salt Marsh and a north-south trending segment separating Fish Lake Valley and northern Clayton Valley (Fig. 6). At the northernmost extent, the eastern Volcanic Hills and northern Silver Peak Range forms part of the narrow (3 to 5 km) east-west topographic divide between Fish Lake Valley and Columbus Salt Marsh (Fig. 6). Moving east from the north-central Volcanic Hills over a distance of about 12 km, the topography decreases from 2,040 m to 1,400 m at a low pass that periodically connected Pleistocene lakes in Fish Lake Valley and Columbus Salt Marsh (Reheis et al., 1993). East of the pass, the northern Silver Peak Range rises from about 1,400 m in the west to 2,000 m in the east over a distance of about 10 km. At the eastern extent of the range, the ridge trends north-south and forms a 3 to 5 km wide topographic high separating northern Fish Lake Valley and northern Clayton Valley. The ridge rises north to south from 2,000 m to about 2,300 m. The north-south trending ridge is bounded to the west by low hills reaching elevations of 1,600 m that extend south along the eastern flank of northern Fish Lake Valley for about 12 km, where the morphology of the mountains changes to the equant-shaped central and southern Silver Peak Range.

The rocks of the northern Silver Peak Range and Volcanic Hills (Figs. 8, 10, and 11) consist of Paleozoic and Cenozoic rocks that are part of the upper-plate assemblage of the SPLM extensional complex (Oldow et al.,1994; 2003; 2009). The upper-plate assemblage contains Miocene volcanic and sedimentary rocks in depositional contact with Paleozoic rocks and Oligocene tuff in structural contact with underlying Paleozoic rocks. The Miocene and Oligocene sections are observed in depositional contact at only two locations, and together with Paleozoic strata, all are overlain by Pliocene to Quaternary basalt and volcaniclastic rocks. The SPLM detachment is exposed as a northwest-trending doubling-plunging anticline exposing metamorphic tectonites of the lower-plate assemblage (Oldow et al., 2003) in the central Silver Peak Range (Fig. 6). At the westernmost exposures, the SPLM detachment dips 10° to the northwest and projects beneath the northern Silver Peak Range. At the range-front 11 km to the northwest, the SPLM detachment fault and lower-plate rocks are intercepted at a depth of 1 km in a geothermal exploration well (Hulen et al., 2005).

4.2 Lithology of the northern Silver Peak Range and Volcanic Hills

In the northern Silver Peak Range and Volcanic Hills, pre-Cenozoic units are composed of early Paleozoic carbonate and siliciclastic rocks (Robinson et al., 1976) deposited both in shelf-platform environments and in deep basinal conditions (Stewart, 1980; Oldow, 1984). Highly deformed basinal rocks composed of argillite, bedded chert, and thin carbonate beds structurally overlie platform and shelf carbonate and clastic rocks on the shallowly-dipping Roberts Mountain thrust (Oldow, 1984). The thrust was emplaced during the Late Devonian to Early Carboniferous Antler orogeny (Roberts et al., 1958; Stewart, 1980; Johnson and Pendergast, 1981; Speed and

Sleep, 1982), which marked the end of deposition in the Paleozoic miogeosynclinal succession (Oldow et al., 1989; Burchfiel et al., 1992). The Cenozoic rocks are composed of rhyolite and latite ash-flow tuff and flows, andesite, volcaniclastic sedimentary rocks, and basalt (Fig. 8). Pliocene sedimentary rocks and basalt rest unconformably on Paleozoic rocks and on all older Cenozoic units. Late Miocene volcanic and sedimentary rocks have a complex internal stratigraphy characterized by local omission of units and major changes in thickness across the area. Different parts of the late Miocene succession rest unconformably on early Miocene andesite, Oligocene tuff, and Paleozoic strata. In this area, the Miocene andesite is restricted to small outcrops in the Volcanic Hills where it rests depositionally on Oligocene tuff. The Oligocene tuff is part of the regionally extensive Candelaria tuff succession (Speed and Cogbill, 1979) and constitutes the oldest Cenozoic rocks in the area. Unlike exposures in the central Silver Peak Range and elsewhere in mountain ranges to the north, the Oligocene tuffs exposed in the Volcanic Hills and northern Silver Peak Range do not have a depositional base and are only found in structural contact with the underlying Paleozoic basement. The structural contact dips shallowly beneath the tilted tuffs and is part of the Monte Cristo detachment. The upper depositional contact of Oligocene tuff is exposed in two locations; one where it is overlain by Miocene andesite and another where it is overlain by late Miocene volcaniclastic rocks.

Pliocene basalt and volcaniclastic sediments are coeval, at least in part, and are spatially segregated across the region. The basalt succession is locally interbedded with basaltic andesite and is dated by K-Ar at 2.9 to 4.8 Ma (Robinson et al.,1968; Reheis and Sawyer, 1997; Lee et al., 2003). The basalt unit ranges in thickness from 60 to 90 m and blankets the northwestern part of the region. The volcaniclastic sedimentary rocks are part of the Fish Lake Valley assemblage and

have a more spatially restricted distribution (Oldow et al., 2009) within and adjacent to active extensional basins. They unconformably overlie late Miocene volcanic rocks along the eastern flank of the southeastern Volcanic Hills and Oligocene tuffs in the western Silver Peak Range. The Fish Lake Valley assemblage is about 1.3 km thick and consists of interbedded lacustrine to fluvial mudstone and sandstone containing minor conglomerate interbeds overlain by fluvial to alluvial sandstone and conglomerate (Fig. 8). The basal part of the succession rests unconformably on Miocene welded latite tuff dated by $^{40}Ar/^{39}Ar$ at 5.85 to 5.87 Ma, and consists of interbedded sandstone and minor conglomerate locally intercalated with basalt flows dated by $^{40}Ar/^{39}Ar$ at 3.71 to 3.76 Ma (Oldow et al., 2009). The basal section passes upward into interbedded sandstone with occasional conglomerate beds and has a unit thickness of about 750 m. Volcanic ash layers within the Fish Lake Valley assemblage are dated and/or correlated to regionally extensive ash units (Reheis et al., 1993; Sarna-Wojcicki et al., 2005) and provide internal age control. Ash horizons within the lower sequence of interbedded sandstone, mudstone, and minor conglomerate are dated by K-Ar and $^{40}Ar/^{39}Ar$ between 3.4-5.2 Ma near the base and are as young as 2.14-2.22 Ma at the transition with the overlying sandstone-conglomerate unit. The upper sandstone-conglomerate unit is between 300 to 400 m thick. The upper unit exposes an ash bed at the base of the coarse-grained section with an age of 2.0 Ma ($^{40}Ar/^{39}Ar$) and passes up-section to the highest directly dated horizon at 0.74 Ma ($^{40}Ar/^{39}Ar$). The upper age limit of the sandstone-conglomerate unit is not determined directly but predates alluvial deposits with lower age bounds of late middle Pleistocene (Reheis, 1991).

Late Miocene volcanic and sedimentary rocks ranging in age from 13 to 5.85 Ma (Robinson et al., 1968; Oldow et al., 2009) are exposed in the central Silver Peak Range and southeastern

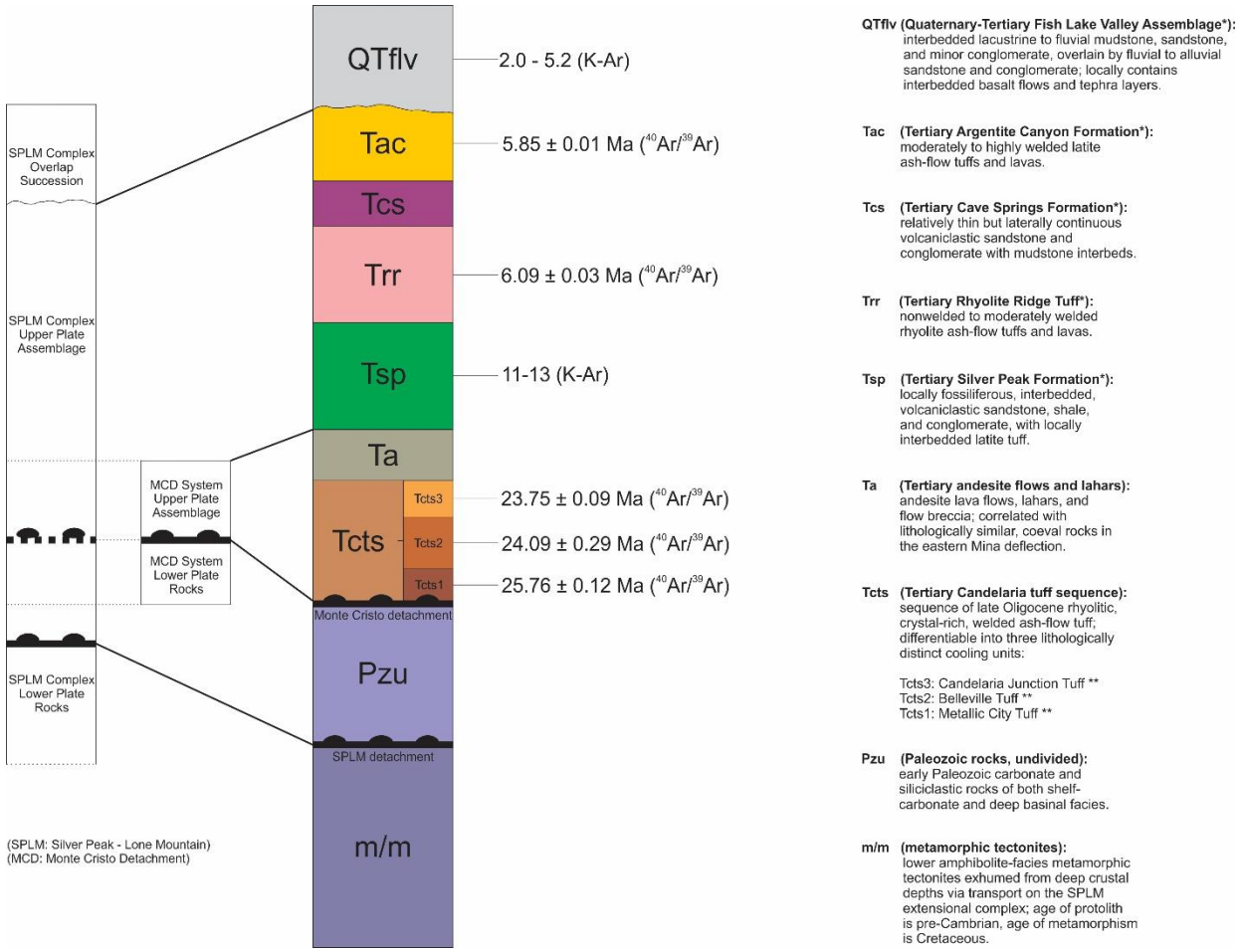

Figure 8. Volcanic stratigraphy and geochronology of northern Fish Lake Valley (northern Silver Peak Range and Volcanic Hills). Units are divided into structural assemblages in the context of the Silver Peak – Lone Mountain extensional complex. The Monte Cristo detachment is contained within the upper plate assemblage of the Silver Peak – Lone Mountain detachment system, and decouples Paleozoic layered rocks from Oligocene ash-flow tuffs and Miocene andesite.

Volcanic Hills and compose a stratigraphic succession characterized by major internal unconformities and profound lateral thickness variations. The lower part of the section consists of interbedded volcaniclastic sandstone, shale, conglomerate, and local interbedded latite tuff known as the Silver Peak Formation (Fig. 8), with an aggregate thickness varying over distances of a few kilometers from a few hundred meters to as much as 2.0 km (Stewart and Diamond, 1990; Oldow et al., 2009). The sedimentary succession rests depositionally both on Miocene andesite and on Paleozoic rocks. The sedimentary rocks are unconformably overlain by volcanic rocks containing minor sedimentary interbeds.

The lower volcanic succession is composed of rhyolite tuff and flows (Fig. 8), known as the Rhyolite Ridge Tuff, dated by $^{40}Ar/^{39}Ar$ as 6.0 Ma (Oldow et al., 2009). The tuff typically has a thickness of 300 m but is locally absent and in some localities reaches a thickness of 435 m. The rhyolite tuff is overlain by volcaniclastic sandstone and conglomerate with interbeds of mudstone of the Cave Springs Formation (Fig. 8) and ranges in thickness from 10 m to 300 m thick (Oldow et al., 2009). Even where thin, the sedimentary succession can be traced laterally for kilometers across the central Silver Peak Range. The volcaniclastic rocks are overlain by latite tuff and flows of the Argentite Canyon Formation (Fig. 8) which have an $^{40}Ar/^{39}Ar$ age of 5.85 Ma, and range in thickness from 30-50 m where they are composed of moderately to highly welded tuff but thicken to 610 m where they are composed of lava flows (Oldow et al., 2009). All late Miocene rocks show dramatic and abrupt changes in thickness across a network of west-northwest and north-northeast trending high- angle faults. The faults form the boundaries of small extensional basins and the stratal geometries and patterns of thickness variations of the sedimentary and volcanic rocks indicate a complex pattern of differential extension. The north-northeast trending faults

localized subsidence and west-northwest faults served as transfer structures, relaying displacement between structural basins as synextensional deposition accompanied northwest-directed transport of the SPLM upper-plate assemblage (Oldow et al., 2009).

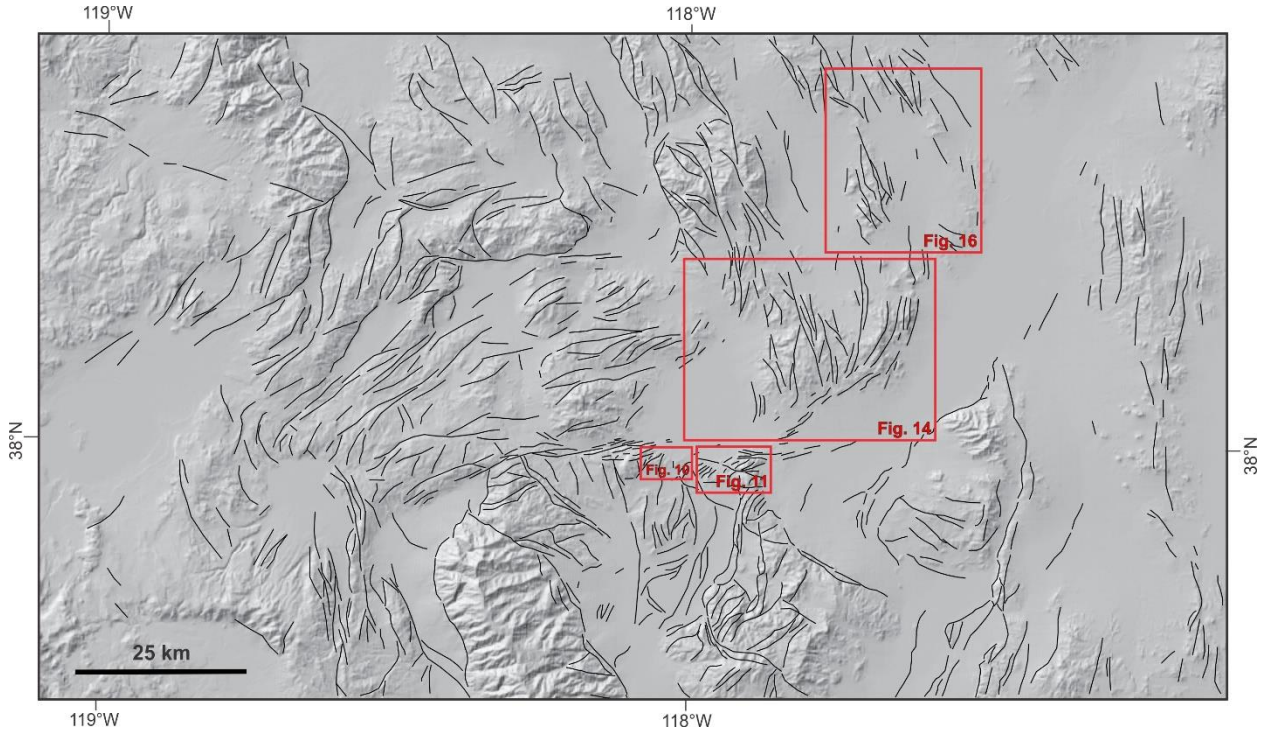

Figure 9. Locations and extents of Figures 10, 11, 14 and 16 outlined in the red boxes, which are geologic maps of the northern Volcanic Hills, northern Silver Peak Range, Monte Cristo Range, and the southern Cedar Mountains and Royston Hills, respectively.

The late Miocene sedimentary rocks of the Silver Peak Formation (Oldow et al., 2009) are exposed in the low-lying hills north of the Silver Peak Range where they rest unconformably on Oligocene ash-flow tuffs of the Candelaria succession. The sedimentary succession is lithologically similar to coeval rocks in the central Silver Peak Range and western Volcanic Hills and is composed of volcaniclastic sandstone, conglomerate, and thin horizons of interbedded latite tuff. The rock types form individual units that are lithologically distinct and range in thickness by a few hundreds of meters (Moore, 1981; Stewart, 1989). The units show minor along-strike changes in thickness but are laterally continuous for several kilometers. An interbedded latite tuff located near the base of the sedimentary succession is dated by K-Ar as 12.7 ± 0.2 Ma (Evernden and James, 1964; Robinson et al., 1968; Stewart, 1989).

In the Volcanic Hills, andesite is exposed in only one area (extreme southwest corner of Fig. 10) and depositionally rests on Oligocene ash-flow tuff. The andesite is about 40 m thick and is itself overlain by late Miocene volcaniclastic sedimentary rocks of the Silver Peak Formation. The andesite is composed of south-dipping flows separated from thick accumulations of the Candelaria tuff sequence to the north by an east-west striking fault that dips about 60° to the south. The andesite is not dated directly but based on correlation with lithologically similar rocks is interpreted to be early to mid-Miocene in age.

The Candelaria tuff sequence is exposed over a region of about 4500 km^2 and is composed of three primary cooling units (Fig. 8), some of which locally constitute compound cooling units. The tuffs are assigned, in ascending stratigraphic order, to the Metallic City, Belleville and Candelaria Junction Tuffs of Speed and Cogbill, 1979 and are dated by $^{40}Ar/^{39}Ar$ as 25.76 ± 0.12 Ma, 24.09 ± 0.29 Ma, and 23.75 ± 0.09 Ma, respectively (Petronis and

Geissman, 2008). In the Volcanic Hills and northern Silver Peak Range, the Candelaria tuffs show substantial changes in thickness laterally. Broad east to west changes in aggregate thickness are observed, with the Candelaria tuffs achieving the greatest thicknesses in the eastern part of the northern Silver Peak Range (430 m) and farther west in the northern Volcanic Hills (335 m) with laterally variable thicknesses of 290 m to 130 m observed in the intervening region.

The Metallic City Tuff is a moderately to densely welded, medium grained, rhyolitic ash-flow tuff which locally displays strongly developed zonation. The Metallic City Tuff forms the base of the Cenozoic stratigraphy and the lower member of the Candelaria Tuff sequence exposed in the northern Silver Peak Range and Volcanic Hills. In these areas, the Metallic City Tuff only sits in structural contact with pre-Cenozoic basement rocks along the Monte Cristo detachment fault (Figs. 10 and 11), but elsewhere in the Mina deflection region, such as in Miller Mountain and the Candelaria Hills (Fig. 6), the tuff is observed to be in depositional contact on pre-Cenozoic rocks and older Cenozoic volcanic rocks. The Metallic City Tuff is depositionally overlain by the Belleville Tuff. The tuff unit forms steep, cliff-like outcrops with crudely developed columnar jointing in a few locations, and the uppermost member of the tuff unit displays an angular to platy weathering habit.

The Metallic City Tuff is characterized by two different volcanic facies from west to east across the northern Silver Peak Range and Volcanic Hills. In the northern Volcanic Hills and the western and central parts of the northern Silver Peak Range, the unit shows strong zonation into a poorly welded basal pumiceous member that locally passes upward into a dark grey vitrophyre, which is overlain by an upper member of varicolored, moderately welded crystallized tuff. The

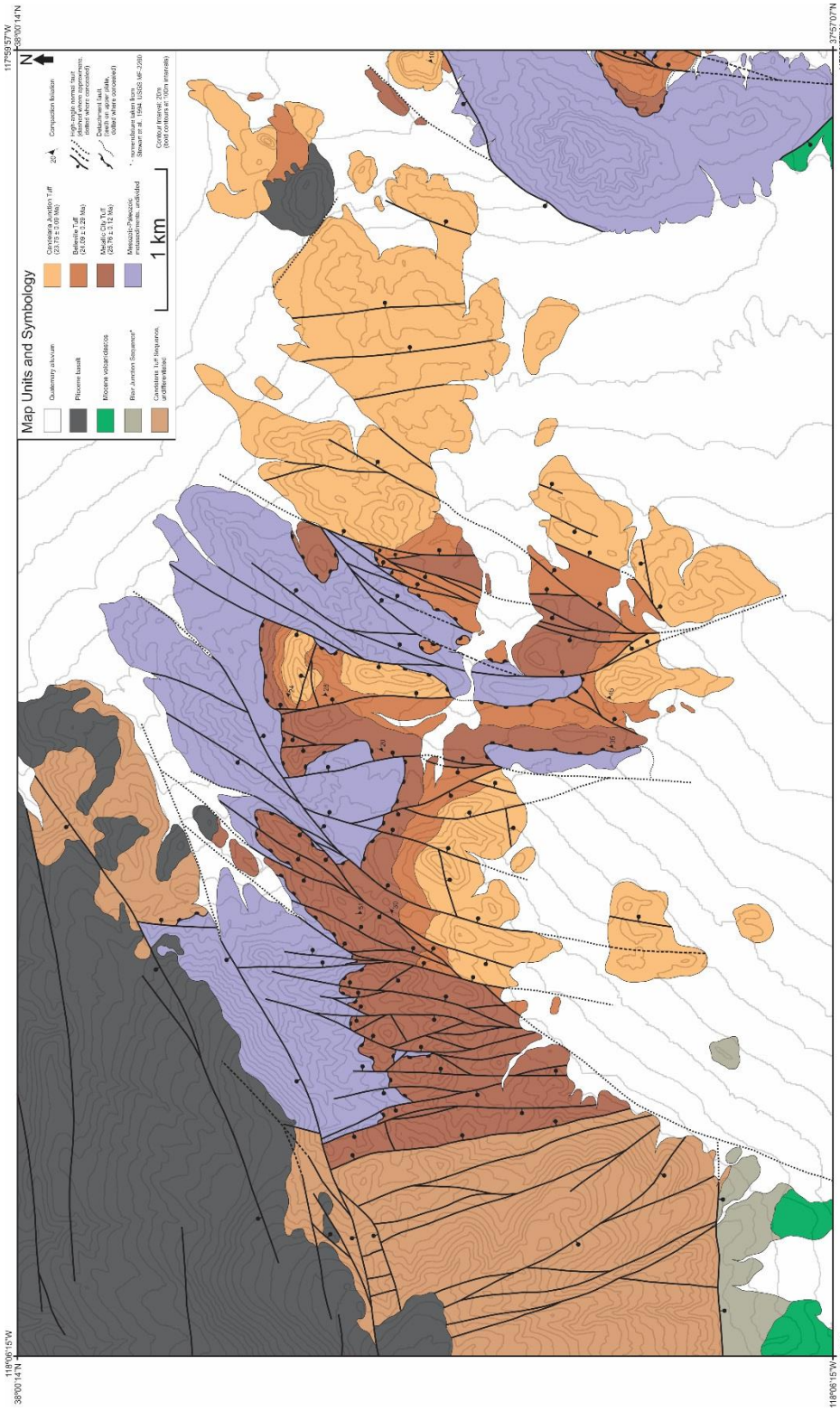

Figure 10. Geologic map of the northern Volcanic Hills.

basal member is white to pale pink and gradually darkens in color and increases in degree of welding moving up-section to the dark grey vitrophyre. The upper crystallized member is varicolored to shades of maroonish to brownish to pinkish-grey, pinkish to reddish-purple and reddish-orange. In the eastern parts of the northern Silver Peak Range, the unit does not display this type of zonation and is entirely glassy and light to medium-grey in color. In these eastern outcrops, the uppermost parts of the Metallic City Tuff locally become pale lavender in color when its depositional contact with the overlying Belleville Tuff is approached up-section. In some locations, the basal parts of the Metallic City Tuff are locally altered to a conspicuous bluish-green color where the unit sits in direct contact with the basement rocks along the detachment, in addition to another type of secondary alteration that takes the form of yellow colored bands and zones that are pervasive throughout the tuff.

Lithic fragments generally constitute about 1-2% of the Metallic City Tuff, but locally can exceed 5%. The lithics range from 1.0 mm to 3.0 cm in length and are composed almost entirely of angular to subrounded pre-Cenozoic metasedimentary clasts, but on rare occasion include clasts of older ash-flow tuff. Pumice usually constitutes less than 5% of the rock, but increases up to 10-15% locally in the dark-grey vitrophyre member. When present, the pumice clasts are rounded and range from 0.5 mm to 1.0 cm in length, but in the vitrophyre member they become highly flattened and up to 2.5 cm long. On average, the tuff unit is composed of 25-45% phenocrysts supported in a moderately welded, highly indurated very-fine ash matrix. Where the unit is strongly zoned, the relative abundance of phenocrysts increases moving up-section from the basal member. The phenocryst population consists of biotite (40-60%), sanidine (15-25%), and quartz (5-20%). Phenocryst size and crystal habit vary for each mineral; euhedral to

subhedral biotite ranges from less than 0.5 to 4.0 mm, euhedral to anhedral sanidine ranges from 0.5 to 4.0 mm, and subhedral to anhedral quartz ranges from 0.5 to 5.0 mm. Biotite is black to dark brown, sanidine is colorless to light grey, and quartz is usually colorless to smoky grey but in some places is yellow or red in color.

The Belleville Tuff is a densely welded, pumice and lithic-rich, rhyolitic ash-flow tuff, which locally constitutes a compound cooling unit. The Belleville Tuff forms the middle member of the Candelaria Tuff sequence in the northern Silver Peak Range and Volcanic Hills, and is more extensively preserved to the east, rather than in the west where the unit is more highly eroded and obscured by Quaternary alluvium (Figs. 10 and 11). The Belleville Tuff sits structurally on pre-Cenozoic rocks along the Monte Cristo detachment fault, sits depositionally on the Metallic City Tuff and is itself depositionally overlain by the Candelaria Junction Tuff. In the northeastern part of the northern Silver Peak Range, relatively thin Quaternary landslide deposits consisting of unconsolidated blocks of ash-flow tuff locally cover the Belleville Tuff (Fig. 11). The tuff unit is typically highly eroded and only preserved as remnant outcrops, but in the eastern domain is observed to form steep cliffs with prominent ledges in its upper member with crudely developed columnar jointing. The Belleville Tuff is characterized by a variety of notably vibrant colors, a heavy degree of welding, an abundance of lithic clasts, and a well-developed compaction foliation formed by lapilli to bomb-sized pumice and glass shards that locally impart a strong eutaxitic fabric to the tuff. In many places, the tuff displays a characteristic weathering habit forming sharp, irregular blocks with a texture that appears to somewhat resemble that of scoria. The sizes of rounded empty cavities in the tuff are the within the same range as pumice and lithic clasts present in the rock, and so this type of texture is more

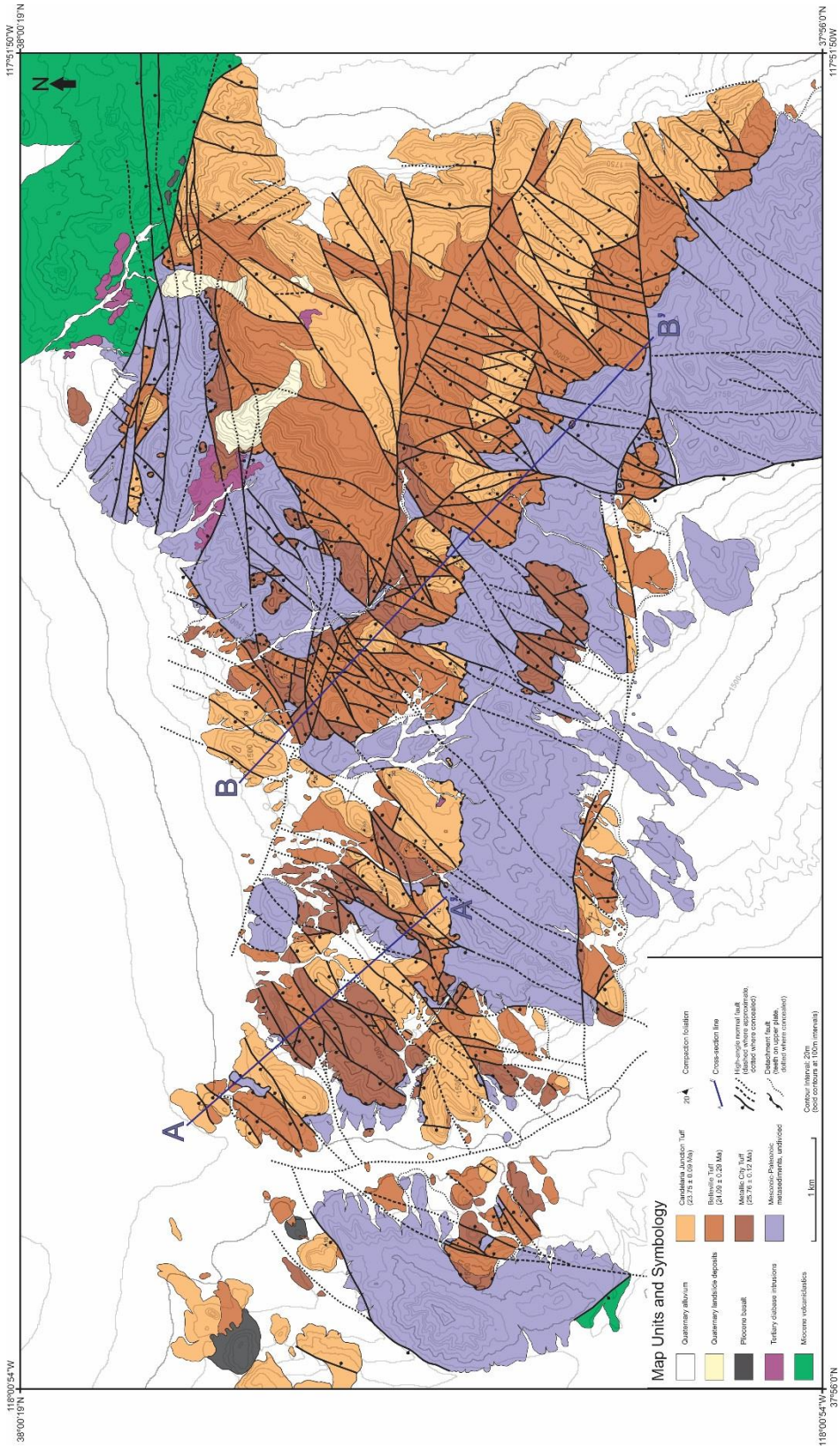

Figure 11. Geologic map of the northern Silver Peak Range.

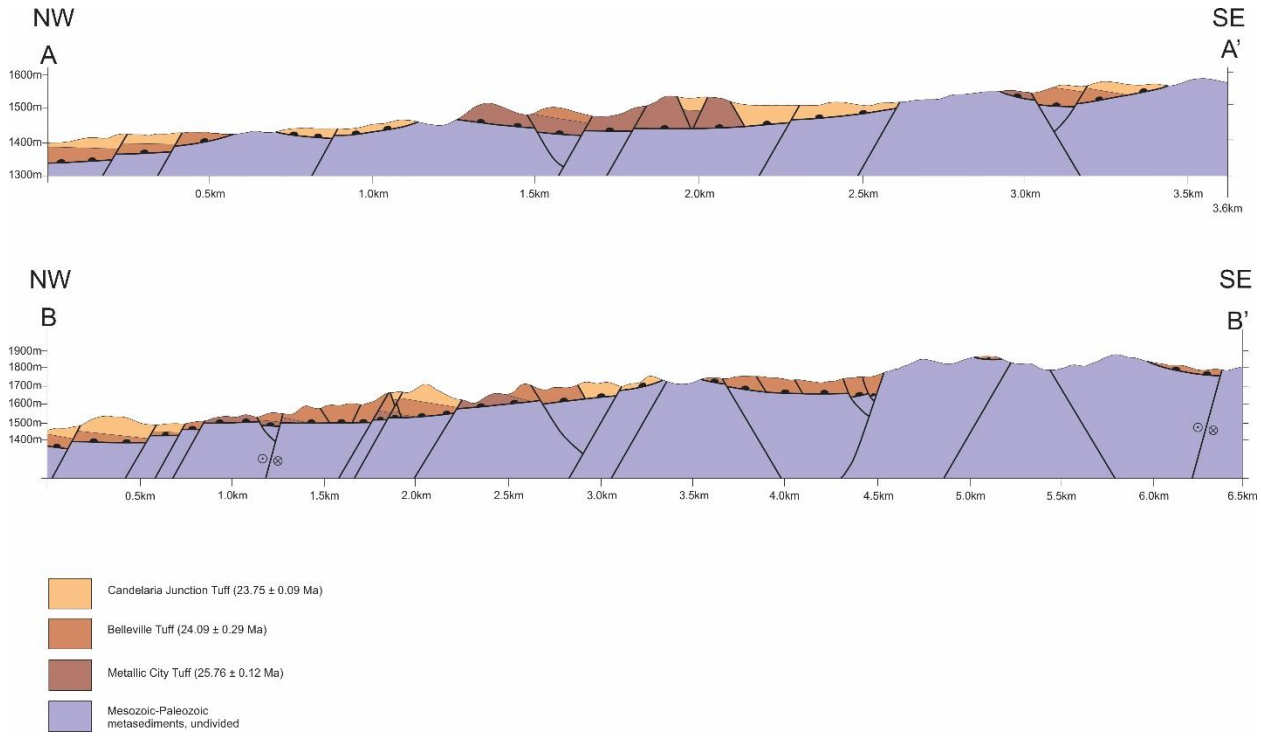

Figure 12. Schematic cross-sections of the northern Silver Peak Range.

than likely to be caused by pumice and lithics weathered out from the tuff following its deposition.

In the west, the Belleville tuff consists of a basal pumiceous member that locally grades upward into dark-grey vitrophyre, which is overlain by an upper crystallized member that is crystal-rich, coarse-grained and variably colored. In the eastern parts of the northern Silver Peak Range, however, the tuff locally becomes a compound cooling unit, composed of two members each with a typical layered structure consisting of a basal pumiceous member, a 10 to25 m thick horizon of locally developed intermediate vitrophyre, and an upper crystallized member. The rocks show the same phenocryst populations and lithic and pumice contents in both the lower

and upper members wherever the Belleville Tuff is a compound cooling unit. Basal members are white in color as well as various pale shades of yellow, pink and light grey. Upper crystallized members are very often vibrant reddish-orange to brick red in color, but are locally varicolored to tannish-white, yellowish-brown, maroonish to reddish-brown and reddish-purple. The uppermost parts of the unit appear to be highly oxidized and weathered to a brownish-black color in many places.

Lithic clasts are abundant in the basal pumiceous member of the Belleville Tuff, typically comprising about 10-20% of the rock near the base and about 5-10% at the top of the unit. Lithics are subangular to rounded, poorly sorted and variably sized, typically ranging from coarse sand to cobble-sized, but can reach up to boulder-size with diameters of up to 35 cm in some places. The lithics consist of altered porphyritic volcanic clasts of older tuffs and andesite. Robinson and Stewart, (1984) described the lithics of the Belleville Tuff as subrounded clasts of porphyritic andesite, and Speed and Cogbill, (1979) described the clasts of the same unit as being composed of older dacitic to rhyolitic welded tuffs and dacitic flows. Pumice constitutes between 10-20% of the rock in the basal member, increases slightly up to 25% wherever the local vitrophyre is present, and is typically between 1-10% in the upper crystallized member. The pumice clasts vary from white to pale pink and tan-colored and are subangular to rounded, ranging in size from 0.5 mm to 3.5 cm long. Wherever the dark grey vitrophyre is present, pumice clasts become highly flattened and take the form of dark grey to black colored, elongate and sometimes sinuous vitric shards which produce a well-developed compaction foliation. The pumice clasts have variable aspect ratios and are typically lapilli to bomb-sized, on average 2.0

mm to 6.0 cm long and 0.5 mm to 1.5 cm wide, but in some places the shards can reach up to 30 cm in length and 7.5 cm in width.

The Belleville Tuff is composed of about 10-45% coarse-grained phenocrysts supported in a moderately to densely welded, highly indurated very-fine ash matrix. The phenocryst population consists of biotite (2-10%), sanidine (20-45%), and quartz (20-45%). Phenocryst size and crystal habit vary for each mineral; euhedral to anhedral biotite ranges from less than 0.5 to 4.0 mm, subhedral to anhedral sanidine ranges from 0.5 to 5.0 mm, and quartz is typically subhedral to anhedral and about 0.5 to 4.5 mm in size, but rare euhedral bipyramids have also been observed. Biotite is black to dark brown, sanidine is colorless to light grey, and quartz is colorless to smoky grey and sometimes pinkish in color.

The Candelaria Junction Tuff is a moderately to densely welded, coarse-grained, rhyolitic ash-flow tuff with well-developed compaction foliation. The Candelaria Junction Tuff forms the upper member of the Candelaria Tuff sequence in the northern Silver Peak Range and Volcanic Hills. The Candelaria Junction Tuff is structurally juxtaposed with pre-Cenozoic basement rocks along the Monte Cristo detachment fault, which is most clearly seen in the west-central and east-central parts of the northern Silver Peak Range (Fig. 11). The Candelaria Junction Tuff depositionally overlies the Belleville Tuff with erosional unconformity, and contacts between the two tuffs are most clearly seen in the western part of the Volcanic Hills and the eastern part of the northern Silver Peak Range (Figs. 10 and 11). The tuff unit forms cliff-like outcrops with poorly developed columnar jointing and displays a characteristic orbicular weathering habit to subrounded blocks.

The Candelaria Junction Tuff characteristically commonly displays strong zonation into several members. The basal member is poorly welded, white in color, and pumice-rich. Moving up-section the basal member shows a gradational increase in the degree of welding and flattening of pumice clasts, as well as a gradual darkening in the colors of the ash matrix and pumice clasts. The basal member locally grades upward into an easily recognizable black vitrophyre with both rounded obsidian nodules and elongate black to brownish-black vitric shards that impart a well-developed eutaxitic fabric to the rock. Overlying the basal member and local vitrophyre is an upper crystallized member which is coarse grained and phenocryst-rich which, despite having a lower pumice content than the vitrophyre, still maintains a well-developed compaction foliation from flattened vitric shards. The upper crystallized member shows variable colors ranging from light to medium brown, tannish-brown, pinkish-brown, greyish-brown, and light grey. The uppermost parts are heavily weathered to dark-greyish brown to brownish-black in some places, and occasionally show intervals of locally intense hematitic alteration with a bright orange color.

The Candelaria Junction Tuff as an entire unit generally has less than 1% lithic clasts. Wherever occasional lithic clasts do appear, however, they are typically granule-sized and are composed of older ash-flow tuffs. The tuff is highly-pumiceous in all members, with 10-30% pumice in the basal member, which gradually increases up-section into the vitrophyre member where pumice contents may reach 40-50%, but decreases to 10-25% pumice in the upper crystallized member. In the basal member, pumice clasts are subangular to rounded, white to light pink in color, and ash to lapilli-sized typically ranging from 0.5 mm to 4.2 cm long. Moving upwards into the black vitrophyre and upper crystallized members, the pumice darkens in color to maroon, dark grey and black, becomes highly-flattened, elongate and sometimes

sinuous and is typically lapilli-sized between 0.5 to 4.0 cm, but in some places can reach upwards of 7.0 cm in length. The Candelaria Junction Tuff is crystal-rich and consists of 40-60% phenocrysts supported in a moderately to densely welded, highly indurated very-fine ash matrix. The phenocryst population is composed of biotite (15-20%), sanidine (20-45%), and quartz (20-50%). Phenocryst size and crystal habit vary for each mineral; euhedral to anhedral biotite ranges from less than 0.5 to 4.0 mm, subhedral to anhedral sanidine ranges from 0.5 to 3.5 mm, and quartz is typically subhedral to anhedral and 0.5 to 4.0 mm in size. Biotite is black to dark brown, sanidine is colorless to light grey, and quartz is colorless to smoky grey.

In the Volcanic Hills (Fig. 10), the aggregate thickness of the Candelaria tuff sequence ranges from 130 m to about 335 m, with the thickest accumulation exposed in the west. Lateral changes in thickness are observed for all tuff members, but in general the thickness gradient for individual units is difficult to assess because the stratigraphy is fragmented and juxtaposed in numerous fault blocks. Fortunately, at one locality (Fig. 10) abrupt changes in unit thickness are preserved across a well exposed array of north-northeast striking and west-northwest to east-northeast striking faults. The structurally linked faults are inactive and are truncated by the underlying Monte Cristo detachment.

The thickness of the Oligocene tuff section changes abruptly across the north-northeast striking pre-detachment fault. On the east side of this fault, a complete section of the Candelaria tuffs has a thickness of 120 m with the lower (Metallic City), middle (Belleville) and upper tuff units (Candelaria Junction) contributing 30 m, 20 m and 70 m, respectively. To the west of this structure, the aggregate thickness of the tuffs increases to 210 m. The lower and middle members

show a three- and two-fold increase in thickness, respectively, with lower member (Metallic City) increasing from 30 m to 90 m and the middle (Belleville) member increasing from 20 m to 40 m. The preserved thickness of 80 m of the upper member (Candelaria Junction) west of the fault is consistent with the observed thickness to the east, suggesting that the structure exerted no control on the accumulation of the upper tuff. About 3 km west, the thickness of the upper tuff member (Candelaria Junction) increases to about 125 m without an obvious increase in thickness of the underlying units. The tuff section also preserves a north-south thickness change across faults. In the section of tuff east of the north-northeast striking high-angle fault, the basal non-welded part of the upper member (Candelaria Junction) shows a north to south increase in thickness from 10 m to 40 m. The thickness increase occurs between outcrops 200 m apart separated by west-northwest and east-northeast striking faults with down-to-the-south displacement. Comparison of north-south thickness variations in the older members of the Candelaria tuff sequence is not possible in this area, however, because the units are structurally omitted to the south by the underlying low-angle detachment. Overall, a one-and-a-half to three-fold increase in individual unit thickness of the Candelaria tuffs is observed across the Volcanic Hills. Abrupt thickness changes are observed for all members across faults that predate the underlying detachment. The lower two members show a two- to three- fold increase in thickness across a north-northwest striking fault, and the upper member shows a four-fold increase in thickness across west-northwest and east-northeast striking faults. In the northern Silver Peak Range (Fig. 11), the Candelaria tuffs show an overall thickening from west to east. In the west, the aggregate thickness of the tuffs is between 200 m to 240 m, increases to 280 m to 300 m in the central part of the mountains and achieves a maximum thickness of about 430 m in the east. Lateral thickness changes are observed

for each of the tuff units, but thickness variations of individual members is difficult to assess because of attenuation and disarticulation by the underlying Monte Cristo detachment and younger high-angle faults. North-south thickness variations in the tuff units are not observed in this area.

The lower member of the Candelaria tuff sequence (Metallic City) shows a variation in thickness from 40 m to 100 m along the east-west axis of the northern Silver Peak Range. The degree to which this lateral variation is due to depositional differences or the result of structural omission by the underlying detachment is difficult to assess. To the west, the tuff typically is between 40 m to 50 m thick and locally reaches a maximum thickness in outcrop of 75 m. In the north-central part of the range, several flat-lying tuff klippe resting on basement rocks are between 30 to 50 m thick (Fig. 11). The thickest exposures occur in the central part of the range are 80 to 100 m, but here as elsewhere sit in structural contact with pre-Tertiary rocks.

The middle member of the Candelaria tuffs (Belleville) has a two- to three-fold difference in thickness, from about 40 to 70 m in the west to about 250 to 260 m in the east, indicating significant lateral changes in accommodation space during deposition. The Belleville Tuff reaches a maximum thickness of about 250 to 260 m in the north-central/northeastern part of the range. This substantially thicker accumulation of tuff is bound on its western side by north-northeast striking fault segments that are cross-cut by younger northeast to east-northeast striking faults which merge with east-west striking faults further north (Fig 11). In the east-central and southeast parts of the range, the Belleville tuff is highly disarticulated by north-northeast to northeast striking and east-northeast to east-west striking faults, and in many places shows significant stratigraphic omission along the detachment, but still maintains minimum preserved thicknesses of at least 120 to 160 m in this area.

The upper tuff unit (Candelaria Junction) varies between 40 to 100 m thick across the northern Silver Peak Range but has an erosional upper contact. Fortunately, the tuff has strong zonation with a basal pumiceous member that grades upward into a black vitrophyre overlain by an upper highly welded member. The black vitrophyre member serves as a useful marker and allows recognition of thickness changes across faults. The vitrophyre is typically 10 to 20 m thick in the western and eastern parts of the mountains but increases thickness in the central and east-central parts of the range to about 40 to 50 m, with a local maximum of 70 m in the east-central part of the mountains. Thickness variations in the vitrophyre occur across arrays of north-northeast to northeast-striking high-angle faults, several of which are truncated by the underlying detachment (Fig. 11).

4.3 Structure of the northern Silver Peak Range and Volcanic Hills

The Coaldale fault system (Stewart, 1988; Oldow, 1992; Lee et al., 2003) runs along the northern flank of the Volcanic Hills and northern Silver Peak Range, and forms the south-central segment of the boundary between the Mina deflection and the southern Walker Lane. Specifically, the mountains expose the structural intersection of the Coaldale fault zone and the horsetail array of structures forming the northern Furnace Creek – Fish Lake Valley fault system (Fig. 5). Faults striking more-or-less east-west are prevalent along the northern parts of the topographic divide and are intersected from the south both orthogonally and obliquely by northwest, north, and northeast striking faults. Faults of all orientations are active and have prominent physiographic expressions and numerous examples of well-preserved scarps in talus and alluvial deposits.

The most conspicuous structures in the northern parts of the hills separating Fish Lake Valley and the Columbus Salt Marsh are east-west to west-northwest trending fault arrays, composed of multiple anastomosing strands. The high-angle faults are conspicuous where they cross-cut Oligocene tuff units, but are more difficult to locate and trace along-strike in Paleozoic units. In the northern Volcanic Hills, the fault zone is well exposed along strike for about 16 km and forms a belt between 2 to 3 km wide (Fig. 5). In the western part of the belt, the fault zone consists of three major strands but ramifies to the east, where up to ten strands show geomorphic evidence of active displacement. Along the southwest margin of Columbus Salt Marsh farther east (Fig. 6), the fault passes into unconsolidated basin fill and is located only sporadically where small scarps in alluvium are found. The fault zone broadens and steps south in the northern Silver Peak Range, where it is divided into three belts separated by 1.5 to 2.5 km. The faults cross the length of the mountain range and extend eastward into the low-lying hills to the northeast and continue into western Big Smoky Valley (Figs. 5, 10 and 11). The individual fault zones are traced for 6 to 10 km, and discontinuously for 20 km. The faults are dominated by a left-lateral to left-oblique sense of displacement and ramify from west to east to form anastomosing networks of oblique-slip faults with strand spacings of about 200 to 300 m. The east-west to west-northwest through-going faults are linked by north to north-northeast striking high-angle faults. The north to northeast faults are dominated by dip-slip displacement and are traced along-strike for 1 to 4 km. The faults typically have a spacing of 100 to 200 m and often bifurcate and splay into multiple strands, with vertical offsets of between 10 to 50 meters.

The fault splays at the northern terminus of the Fish Lake Valley fault system (sensu lato) form a horsetail array that intersects the east-west trending Coaldale fault system for over a

distance of 45 km (Fig. 5). Structures of the Fish Lake Valley fault system consist of four major strands separated by 10 to 15 km, with orientations that shift in a west to east direction from northwest, to north, and north-northeast along the length of the Coaldale fault system. Between the major fault strands, minor faults with spacing of hundreds of meters to kilometers form a network that broadly distributes displacement along the intersection of the two major structural belts.

The physiography of northern Fish Lake Valley reflects the orientation and displacement of the faults in the horsetail array. The relatively low topographic relief of the northeastern parts of the White Mountains, along the northwestern flank of Fish Lake Valley, reflects displacement on northwest-striking faults, named here the Trail Canyon and Sand Spring Canyon faults (Fig. 5). The faults have trace-lengths of over 20 km and intersect the Coaldale fault system at high-angles. The central part of northern Fish Lake Valley is terminated by the Volcanic Hills, where Cenozoic and Paleozoic rocks are exposed in the highlands. The northern part of the hills are dissected by a north-south striking fault, named the Volcanic Hills fault, which separates Oligocene tuff to the east from interbedded Miocene volcaniclastic and volcanic rocks to the west. Stratigraphic separation across the Volcanic Hills fault indicates several kilometers of right-lateral displacement and hundreds of meters of down to the west dip-slip motion. At the north end of the Volcanic Hills fault, near its intersection with the Coaldale fault system, Pliocene basalt overlaps the structure but is itself cut by the fault with displacements of tens of meters. The fault is traced south for over 10 km and is observed to cut Quaternary to Holocene talus and alluvium. The Volcanic Hills fault is traced southward into northern Fish Lake Valley for another 20 km on the basis of topographic juxtaposition and steep subsurface gradients determined from detailed gravity studies

(Mueller et al., 2016b). The eastern strands of the northern Fish Lake Valley fault array trend north-northeast and bound deep basins underlying playa deposits east and south of the Volcanic Hills and northwest of the central Silver Peak Range (Fig. 6). The Emigrant Peak fault (Reheis, 1991), has a well-preserved alluvial scarp of up to 30 m high (Fig. 5) and three more faults mimicking the curvilinear trace of the Emigrant Peak fault are found within the western Silver Peak Range (Reheis, 1991; Oldow et al., 2009). To the west, faults within and bounding the northern Fish Lake Valley basins are assigned to The Crossing fault system (Fig. 5) and are located both by physiographic expression and by gravity studies (Mueller et al., 2016b). The curvilinear faults of northeastern Fish Lake Valley form a complex network ranging from 6 to 10 km wide and extend northeast to the highlands of the east-west segment of the northern Silver Peak Range. At the northern boundary, fault displacement is accommodated by numerous splays and west-northwest striking transfer faults as the north-northeast fault array intersects the east-west belt of structures which form the eastern part of the Coaldale fault system.

The northern part of the Emigrant Peak fault forms a horsetail array with west-northwest, north-northwest and north-northeast striking fault strands (Figs. 5 and 11). As the east-west structures of the northern Silver Peak Range are approached from the south, displacement is transferred to a west-northwest striking fault that bounds the northern end of the Fish Lake Valley playa and to several northeast-striking strands that transfer displacement across the topographic divide into northern Clayton Valley. The residual displacement is carried north into the east-west segment of the range, where the Emigrant Peak fault cross-cuts the southern strand of the Coaldale fault system but ramifies into north-northwest, north-northeast, and northeast strands where it

merges with the central strand of the fault zone. At its northern terminus, the Emigrant Peak fault has a cumulative vertical offset of about 150 to 170 m (Fig. 11).

Low-angle detachment faults separating Oligocene tuff from the underlying Paleozoic basement are found in the Volcanic Hills and northern Silver Peak Range (Figs. 10, 11 and 12) and are part of the Monte Cristo detachment. The detachment faults variably dip north and south from sub-horizontal angles up to 20 degrees and are traced along-strike for up to 15 km. The low-angle faults are not planar but rather undulate about west-northwest and north-northeast to north-south axes in low amplitude (hundreds of meters) and long half-wavelength (2 to 10 km) folds. The low-angle faults juxtapose all three members of the Candelaria tuff sequence with Paleozoic basement and in several areas are well exposed, with compaction foliation in overlying tuffs dipping moderately to steeply into the underlying structural contact with Paleozoic rocks. Basement rocks beneath the fault have cataclastic fabrics tens of meters thick in several locations, particularly where the lower-plate is composed of carbonate or interbedded argillite and chert.

The low-angle faults are cross-cut and offset by tens to hundreds of meters by the younger structures of the Fish Lake Valley and Coaldale fault systems, but in several locations high-angle faults are truncated by the underlying detachment. In the northern Silver Peak Range, several north-northeast to north-south striking high-angle faults in the central, east-central and southeast parts of the range are truncated by the detachment (Figs. 11 and 12). The faults are traced along-strike for up to 2 km and form arrays of anastomosing structures with spacing of about 100 to 200 m. The north-northeast striking, pre-detachment faults show vertical offsets of tens of meters where they juxtapose different units of the Candelaria tuff sequence with variable thicknesses. In the central part of the northern Volcanic Hills (Fig. 10), north-northeast, northeast, and west-

northwest striking high-angle faults are abruptly truncated by the detachment. Two north-northeast striking faults, separated by about 325 m are traced north-south for nearly 1 km and vary along-strike from a single strand to multiple splays in fault zones up to 100 m wide. The north-northeast striking faults are well exposed on the sub-vertical face of a canyon and are traced down-dip for 90 m to where they are truncated by the shallowly (< 10°) north dipping detachment fault. Paleozoic rocks beneath the detachment are brittlely deformed and hydrothermally altered to depths of 30 m below the low-angle fault. The decapitated high-angle faults show vertical offsets of less than 20 m, which largely can be explained by the juxtaposition of coeval tuffs of different thicknesses. The easternmost north-northeast striking fault zone is linked to west-northwest and east-northeast trending high-angle faults that have down to the north and down to the south displacement. The east-northeast fault has a curved trajectory where it merges with the north-northeast striking fault zone to the west. Similarly, the west-northwest structure ramifies into an array of three strands that merge with the north-northeast fault zone to the west. The east-northeast and west-northwest faults are truncated to the east by the underlying low-angle detachment.

Timing constraints for activity on the low-angle detachment is not well established in this area. The detachment clearly post-dates the deposition of the Oligocene tuffs (as young as 23 Ma) and predates deposition of the unconformably overlying Pliocene basalt. The limited exposure of the Candelaria tuff overlain unconformably by late Miocene clastic rocks (13-10 Ma) in the low hills northeast of the Silver Peak Range suggests cessation of low-angle faulting by the mid-Miocene. Unfortunately, the exposures in this area are not adequate to conclusively make this determination. Similarly, the thin andesite depositionally overlying Oligocene tuff in the Volcanic Hills does not provide useful timing constraints.

CHAPTER 5

THE MONTE CRISTO RANGE, ROYSTON HILLS, AND CEDAR MOUNTAINS

5.1 Introduction

The morphology of the Monte Cristo Range, southern Cedar Mountains, and the Royston Hills reflects the change in trajectory of active high-angle faults in the eastern Mina deflection. The Monte Cristo Range trends east-northeast for about 25 km and forms the northern margin of western Big Smoky Valley (Fig. 6). The mountains have two topographic highs of about 2300 m in the west and east separated by a modest north-south depression with elevations of about 1900. The western Monte Cristo Mountains gradually decrease in elevation to the north over 15 km, reaching a low of about 1700 m, and then rise to merge with the southern Pilot Mountains, which has a maximum elevation of 2800 m. The eastern topographic lobe shows a similar pattern with elevations diminishing over 10 km to the north to 1700 m before rising to just over 2100 m in the southern Cedar Mountains. The depression between the two topographic highs continues north for 20 km with elevations gradually decreasing to 1650 m at Kibby Flat, the southern end of Monte Cristo Valley (Fig. 6), where bedrock is no longer exposed. The Monte Cristo Valley, separates the Pilot and Cedar Mountains, stretches north for 30 km, and is up to 10 km wide. Farther to the east, the Royston Hills rise from Big Smoky Valley at the latitude of the southern Cedar Mountains and trend north for 20 km, where they swing north-northwest in orientation and extend for another 20 km. The Royston Hills have subdued topography with elevations reaching nearly 1700 m in the south but gradually rise to 1950 m in the north. The hills are separated from the southern Cedar

Mountains by Cirac Valley and form the western boundary of Big Smoky Valley as it curves from east-northeast to north-south.

Rocks of the Monte Cristo Range, southern Cedar Mountains and Royston Hills consist of Paleozoic and Mesozoic strata, Mesozoic plutons, and Cenozoic volcanic and sedimentary rocks. The Cenozoic stratigraphy ranges in age from Oligocene through late Miocene and preserves one of the most complete depositional records in the region (Fig. 13). As such, the area provides some of the best constraints for establishing the timing of deformation during Cenozoic tectonism. The pre-Cenozoic rocks are exposed as structural windows through the Cenozoic cover and form north to northwest-trending structural domes with Cenozoic rocks flanking and locally exposed as isolated exposures at or near the apex of the basement highs. Based on new geologic mapping, the basement assemblage is separated from Oligocene and lower Miocene rocks by a low-angle detachment system and are overlain unconformably by upper Miocene rocks. The detached and unconformably overlying Cenozoic section are deformed together with the pre-Cenozoic basement rocks along active high-angle faults with curvilinear traces.

5.2 Lithology of the Monte Cristo Range, Royston Hills, and Cedar Mountains

Pre-Cenozoic rocks consist of lower and upper Paleozoic carbonate, siliciclastic, and volcanic rocks and lower Mesozoic clastic rocks. The lower Paleozoic rocks yield fossils with Cambrian through Devonian ages and are part of the Roberts Mountains allochthon (Stewart, 1980; Oldow, 1984). The lower Paleozoic siliciclastic rocks are composed of thinly bedded chert, argillite, shale, and minor amounts of sandstone and thin-bedded to massive limestone. Sandstone is rare and is composed of fine- to coarse-grained quartzite. Volcanic rocks are highly altered and

consist of mafic breccia and some pillow lava. Fossils from sedimentary interbeds within the volcanic rocks are early Paleozoic in age. The upper Paleozoic units are carbonate rocks interpreted to be part of the overlap sequence resting on the Roberts Mountain allochthon (Stewart et al., 1994) and thin-bedded clastic and volcaniclastic rocks assigned to the upper plate of the Golconda thrust (Speed, 1984). The upper Paleozoic parautochthonous succession contains thick-bedded limestone and dolomite that contain lower Carboniferous fossils. Although interpreted as part of the depositional overlap sequence resting on the Roberts Mountains allochthon, in this region the upper unit is everywhere in low-angle fault contact with underlying lower Paleozoic rocks (Stewart et al., 1994). Upper Paleozoic clastic rocks are part of the upper-plate assemblage of the Golconda thrust, which was emplaced during the latest Permian and early Triassic (Speed, 1977, 1984). The clastic rocks are composed of thin-bedded chert, volcaniclastic arenite, argillite, and minor silty limestone. The units yield fossils of Carboniferous to Devonian age (Speed, 1984; Stewart et al., 1994) and have sedimentary structures indicative of basinal depositional conditions. The Paleozoic rocks are unconformably overlain by coarse- to fine-grained clastic rocks of the Jurassic Dunlap Formation (Ferguson et al., 1953). The Mesozoic clastic rocks consist of volcaniclastic sandstone and shale interbedded with chert-pebble conglomerate and breccia, with abundant quartz arenite in the lower part of the succession. The layered rocks yield Early Jurassic ammonites and pelecypods (Silberling and Tozer, 1968), and are locally intruded by Jurassic granitic plutons (John, 1987; John and Robinson, 1989). The pre-Cenozoic rocks are exposed as east-west trending belts with successively younger rocks exposed farther north. In the Monte Cristo Range, lower Paleozoic clastic and volcanic rocks of the Roberts Mountains allochthon are found throughout the mountains and are locally overlain by upper Paleozoic carbonate and clastic

rocks, which are assigned to the lower- and upper-plates of the Golconda thrust, respectively. In the southern Royston Hills, upper Paleozoic rocks of the Golconda allochthon constitute the pre-Cenozoic basement, with the same upper Paleozoic rocks exposed in the southern Cedar Mountains. In the Cedar Mountains, the upper Paleozoic rocks are unconformably overlain by Jurassic clastic rocks, which are part of the Mesozoic overlap succession resting on the Golconda allochthon and represent the footwall assemblage to the Mesozoic Luning-Fencemaker thrust system (Oldow, 1983, 1984).

Late Miocene basalt and rhyolite, both dated by K-Ar as 7.2 Ma (Stewart et al., 1994), are the youngest Cenozoic rocks in the area. The basalt rests unconformably on older Cenozoic rocks as a thin blanket up to 50 m thick. The basalt is exposed discontinuously as an east-west trending belt 15 km wide and 45 km long that crosses the northern Monte Cristo Range and southern Royston Hills. Rhyolite is exposed in the southeastern Monte Cristo Range along the range-front with Big Smoky Valley and as a few isolated outcrops on the southeastern slopes of the eastern topographic dome. The rhyolite is composed of flow banded domes and vitrophyre locally overlying tuffaceous sedimentary rocks and tuff breccia.

Cenozoic volcanic and sedimentary rocks form a stratigraphic succession typical of the region (Oldow et al., 2009) and consist of upper Oligocene to lower Miocene rhyolite and andesite volcanic rocks passing upward into late Miocene volcaniclastic sedimentary units (Fig. 13). All of the older units are overlain by regionally extensive late Miocene basalt and spatially restricted rhyolite domes and flows. Across most of the region, this stratigraphic succession must be reconstructed from fragmentary evidence, but in the Monte Cristo Range the stratigraphy is

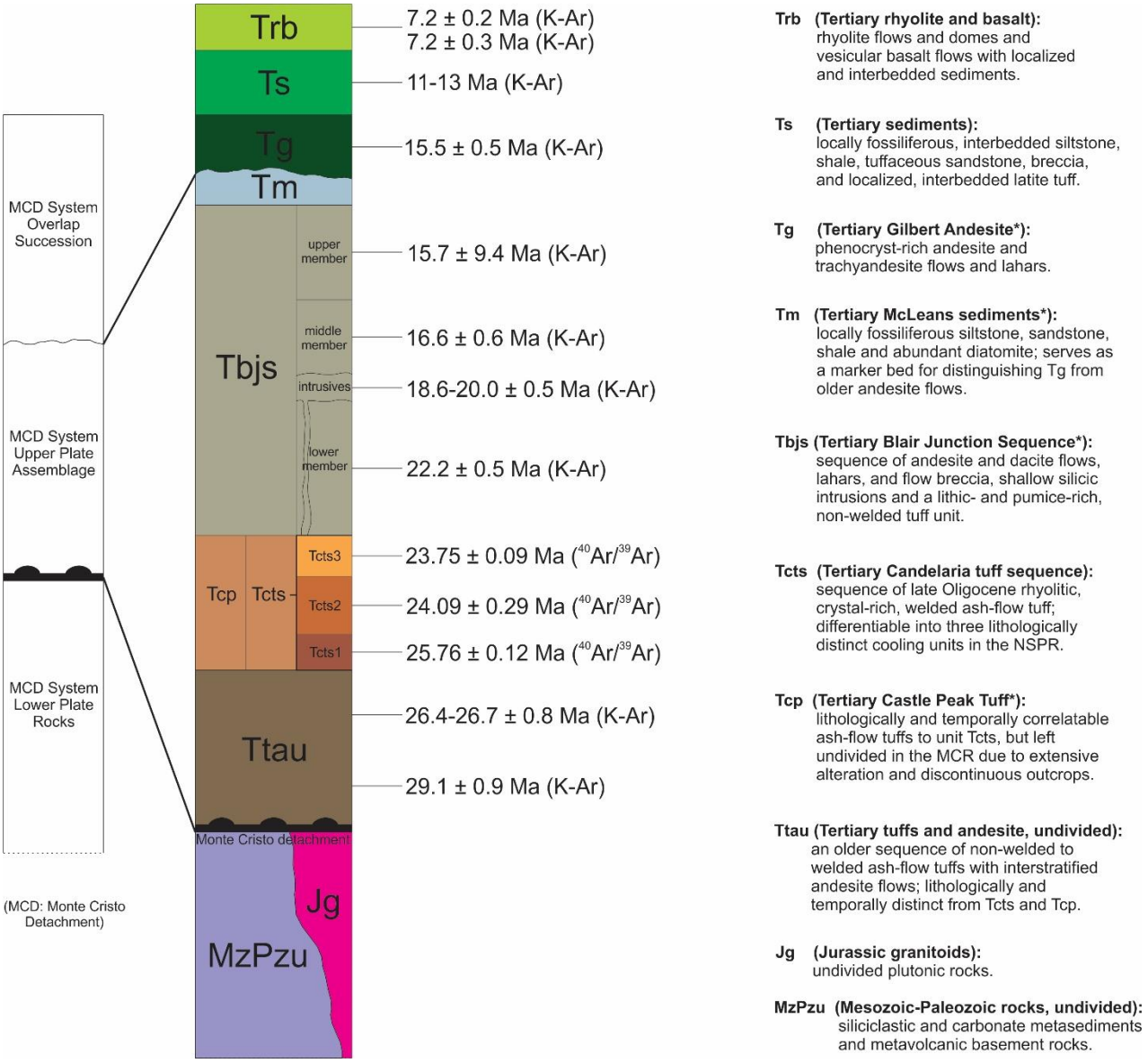

Figure 13. Volcanic stratigraphy and geochronology of the eastern Mina deflection (Monte Cristo Range, Royston Hills, and Cedar Mountains). Units are divided into structural assemblages of lower/upper-plate rocks, and a post-detachment overlap succession that seals the Monte Cristo detachment.

preserved in a relatively intact vertical succession. The Cenozoic rocks are divided into two stratigraphic sequences separated by an angular unconformity. The lower sequence is composed of late Oligocene and early Miocene rhyolite tuff and andesite; the upper sequence consists of mid-Miocene andesite and volcaniclastic sedimentary rocks, all of which are overlain unconformably by late Miocene basalt and rhyolite (Fig. 13).

Late Miocene volcaniclastic rocks have widespread exposure in two belts (Fig. 14). They underlie the low-hills connecting the northeastern Silver Peak Range and the southwestern Monte Cristo Range and are exposed in the topographic depression between the northeastern Monte Cristo Range and southern Cedar Mountains. The southern belt, between the northern Silver Peak and Monte Cristo Ranges, consists of a well exposed succession of shale, sandstone and conglomerate up to several tens of meters thick. The aggregate thickness of the late Miocene sedimentary rocks in this area is about 1.3 km (Stewart, 1989). The northern belt of outcrops between the Monte Cristo Range and Cedar Mountains are not as well exposed, but contain interbedded volcaniclastic sandstone, siltstone, and conglomerate together with sparse limestone. The unit thickness is difficult to assess in this area, because of poor exposure and the possibility of unrecognized structural repetition, but probably exceeds 500 m and may be as much as 1.0 km thick. In the area adjacent to the northern Silver Peak Range, the late Miocene sedimentary rocks overlie late Oligocene tuffs of the Candelaria sequence with angular unconformity and rest on early Miocene andesite along the southern flank of the Monte Cristo Range. In the northern belt of exposures, the sedimentary rocks overlie Oligocene tuff with probable angular unconformity.

The basal unit of the upper stratigraphic sequence is known as the Gilbert Andesite (Ferguson et al., 1953) and is composed of dark, crystal-rich andesite lava and lahar deposits dated

by K-Ar as 15 Ma (Stewart et al., 1994). The unit crops out as massive resistant ledges capping the topographically highest parts of the Monte Cristo Range, where it reaches thicknesses of up to 150 m. The andesite is absent in the northwestern Monte Cristo Range, southern Cedar Mountains and southern Royston Hills (Figs. 14 and 16).

The older stratigraphic sequence consists of a succession of andesite flows, lahar deposits, a medial lithic-rich, nonwelded tuff unit, and minor interbedded sedimentary rocks (Fig. 13). The sedimentary rocks represent a minor part of the stratigraphic section, which is dominated by two andesite successions and an intervening rhyolite ash-flow tuff. The upper andesite and rhyolite tuff are found in the Monte Cristo Range and Royston Hills and the lower andesite and rhyolite tuff are exposed in the northern parts of the Cedar Mountains and the Royston Hills. In the southern part of the region, the rhyolite tuff and upper andesite rests on Paleozoic rocks above a shallowly dipping structural contact. Farther north, Paleozoic and Mesozoic strata are structurally overlain by the lower andesite and rhyolite tuff succession, and the upper andesite succession is not exposed in this area. The lack of exposure of the lower andesite in the southern part of the region is unresolved and may be either the result of non-deposition or structural omission by the underlying detachment. The uppermost stratigraphic unit of the lower sequence of Cenozoic rocks consists of a thin sedimentary unit (less than 30 m thick) composed of interbedded siltstone, shale, shale-rich sandstone, and diatomite (Fig. 13). The clastic unit, known as the "McLean's sedimentary unit" (Stewart et al., 1994), is laterally discontinuous but where preserved serves as an easily-recognized stratigraphic marker. The unit is found in most parts of the southern Monte Cristo Range but appears to be absent or unrecognized elsewhere in the region.

The first regionally significant unit of the lower Cenozoic sequence is an intercalated succession of andesite flows and lahar deposits overlain by non-welded tuff that passes upward into andesite breccia, flows and lahar deposits. This heterolithic andesite unit is known as the "Blair Junction Sequence" (Hambrick, 1984; Stewart et al., 1994) and is found throughout the Monte Cristo Range, but is not observed in the Cedar Mountains or Royston Hills. Recognition of this unit and its segregation from the overlying mid-Miocene Gilbert Andesite by Stewart et al., (1994) was a critical element in our recognition of the two stratigraphic sequences and the existence of the Monte Cristo detachment. The lower part of the andesite succession is very complex and contains flows of different composition, minor sedimentary rocks, and local hypabyssal intrusive rocks. Intrusive rocks of intermediate composition near the base of the Blair Junction Sequence yield a K-Ar age of 22.2 Ma (Stewart et al., 1994), which provide a minimum age for the basal member. The lower member is also intruded by a rhyolite-dacite dome dated by K-Ar as 18-20 Ma (Fig. 13). The thickness of the lower unit is largely unknown because of the internal lithologic complexity and due to the fact that, with few exceptions, the basal unit rests on the detachment fault. The thickest preserved section of the lower unit is 90 m thick, but the lower contact is structural. The lower unit passes upward into lithic-rich non-welded tuff and minor sedimentary rocks. The tuff member has a thickness of at least 100 m and is dated by K-Ar as 16.6 Ma (Stewart et al., 1994). In several locations, where the lower member has been structurally omitted, the tuff member rests directly on Paleozoic rocks. The tuff member is locally overlain by volcaniclastic conglomerate, sandstone, and siltstone as it passes upward into the overlying succession of andesite flows, breccia, and lahar deposits. The upper andesite is at least 100 m

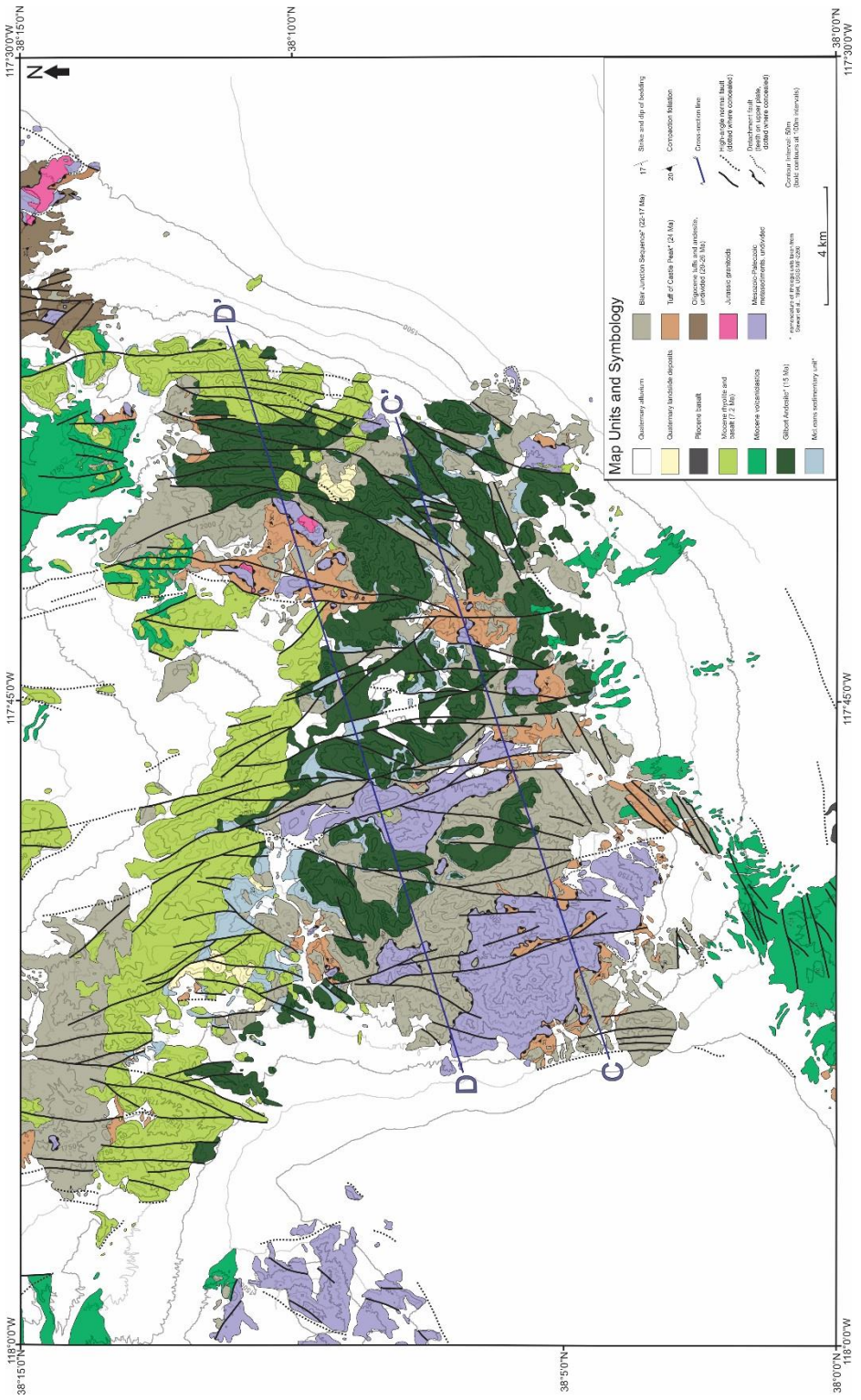

Figure 14. Geologic map of the Monte Cristo Range. Modified from Stewart et al., 1994, USGS MF-2260.

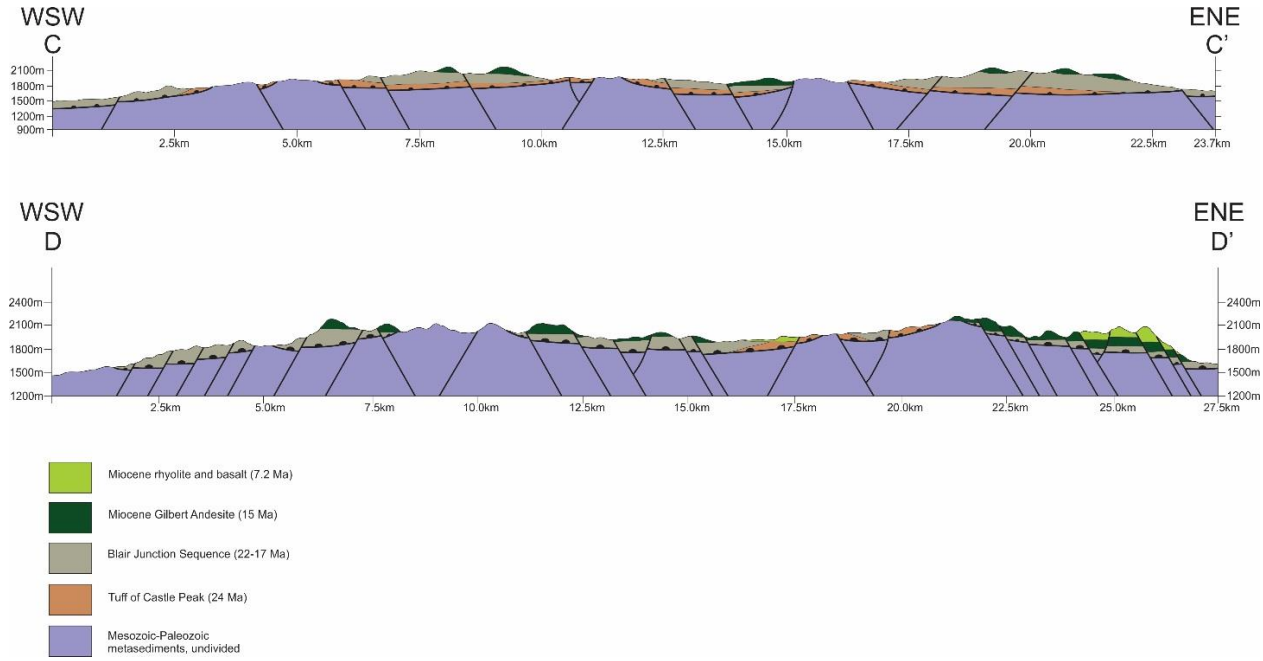

Figure 15. Schematic cross-sections of the Monte Cristo Range.

thick, but the top is highly eroded beneath the overlying Gilbert Andesite. The age of the upper unit is very poorly constrained (Fig. 13) but is younger than 17 Ma and older than 15 Ma.

In the Monte Cristo Range, southernmost Cedar Mountains, and Royston Hills, the oldest part of the lower sequence is composed of rhyolite ash-flow tuff. In the Monte Cristo Range, Oligocene tuff referred to as the "Tuff of Castle Peak" is dated by K-Ar at about 24 Ma but contains additional unmapped and undated cooling units (Hambrick, 1984; Stewart et al., 1994). The unit is highly disarticulated and altered, and contains large blocks of pre-Cenozoic basement in fault-bounded blocks. The tuff everywhere rests on the underlying detachment (Fig. 14) and attains a maximum preserved thickness of about 90 m. The tuff is age equivalent, at least in part, and

probably correlates with the Candelaria tuff succession exposed 12 km southwest in the northern Silver Peak Range. In the Royston Hills and southern exposures of the Cedar Mountains, Oligocene tuffs are also exposed but are lithologically and temporally distinct from cooling units of the Candelaria succession. In these areas, rhyolite to dacite ash-flow tuff consists of at least five cooling units, commonly separated by thin andesite flows, and have K-Ar ages of 26 to 29 Ma (McKee and John, 1987). The units structurally overlie Paleozoic and Mesozoic basement rocks on the shallowly dipping detachment (Fig. 16), but in the Cedar Mountains, also rest depositionally on an older andesite succession which constitutes the lowermost member of the Cenozoic stratigraphy in this area. The older succession is composed of several tens of meters of andesite flows, breccia and lahar deposits. The Oligocene andesite unit underlies an ash-flow tuff dated by K-Ar as 29.1 Ma, but is itself undated.

5.3 Structure of the Monte Cristo Range, Royston Hills, and Cedar Mountains

Active faults in this part of the Mina deflection systematically change orientation, in a west to east direction, from east-northeast through north-south to north-northwest. The faults in the Monte Cristo Range, Cedar Mountains, and Royston Hills are linked to different fault systems within the Mina deflection that transfer displacement from the northern part of the Eastern California shear zone and southern Walker Lane. The structures that dissect the southern Monte Cristo Range are linked to the eastern segment of the Coaldale fault system. In contrast, faults of the northwestern Monte Cristo Range are connected to east-northeast striking faults passing north

of Columbus Salt Marsh in the eastern Candelaria Hills (Fig. 6). The structures in the Royston Hills transfer displacement from the eastern part of the southern Walker Lane.

High-angle faults of the southern Monte Cristo Range are kinematically linked to the east-northeast striking Coaldale fault system. From the southwest, the Coaldale fault system is traced eastward into the low hills separating the northern Silver Peak Range and Monte Cristo Range and into western Big Smoky Valley. The fault strands within the fault zone gradually changes orientation from east-northeast to northeast as the Monte Cristo range is approached from the south. Northeast-striking faults mark the southern margin of the Monte Cristo Range before changing strike orientation to north-south as they cross the range. The southern Monte Cristo Range is crossed by two belts of faults, each about 15 km wide, that emerge to the north as structures bounding and dissecting the eastern Pilot Mountains and southern Cedar Mountains (Figs. 6 , 14 and 16).

East-northeast striking faults exposed discontinuously north of Columbus Salt Marsh and within the southern Candelaria Hills track east into the northwestern Monte Cristo Range (Fig. 6). The east-northeast striking faults change strike to northeast in the eastern part of the Candelaria Hills and to north-south in the northwestern Monte Cristo Range. The faults from a belt of structures about 7 km wide and in the Monte Cristo Range gradually change orientation to north-northwest over a distance of about 15 km, as the structures enter and cross the western Pilot Mountains. In the Pilot Mountains, the main strands of the system form the Pilot Mountain fault and the Dunlap Canyon fault passing across the center of the range (Fig. 5).

North-south striking faults in the southern Royston Hills are not linked to the Coaldale fault zone or the structures in the Monte Cristo Range. Rather, they are the structural continuation of

northeast-striking faults along the southern margin of western Big Smoky Valley and north-south striking faults along the eastern flank of Lone Mountain (Fig. 6). Active faults (Hoeft and Frankel, 2010) separating western Smoky Valley from the Weepah Hills and Lone Mountain to the south strike northeast for 25 km before swinging to north-south orientations, where they are traced a short distance into the basin on the basis of discontinuous scarps in alluvium. The actual structural link across this part of Big Smoky Valley is obscured by a broad swath of active fluvial channels, and faults reemerge in the Royston Hills 18 km to the north. Only a few faults can be located with confidence in the southern Royston Hills, but the structures become more pronounced to the north.

The Monte Cristo detachment fault separates Oligocene to early Miocene rocks of the lower Cenozoic stratigraphic sequence from underlying Paleozoic and Mesozoic rocks throughout this region. The low-angle fault is exposed in northwest-trending structural domes cored by basement rocks (Figs. 14, 15 and 16). The basement highs range from small exposures of only a few square kilometers to large expanses 10 km long and 2 to 5 km wide. The detachment fault dips shallowly (< 20°) away from the axis of the domes. Where undisturbed by younger high-angle faults, the structural domes are doubly plunging anticlines, with amplitudes of about 100-200 m and half wavelengths of between 5 to 10 km.

Oligocene tuff and andesite and lower Miocene andesite rest structurally on the Monte Cristo detachment (Fig. 15). In the southern Monte Cristo Range, exposures of the Oligocene tuff are highly disrupted, sheared, and commonly show substantial hydrothermal alteration. Tuff thickness varies from thin selvages beneath the overlying lower Miocene andesite in the southwest to thick accumulations in the northeast. The distribution of lower Miocene andesite shows substantial differences in thickness across the range. In the western Monte Cristo Range, the lower

parts of the andesite unit are progressively removed from west to east until only the thin section of the McLean's sedimentary rocks are observed to dip into and overlie the underlying detachment fault. In the Royston Hills (Fig. 16), the detachment is areally extensive and shows only minor disruption by younger high-angle faults. In this area, large tracts of Oligocene tuff with compaction foliations of up to 55° overlie and dip into the underlying detachment. In the Cedar Mountains, younger high-angle faults severely disrupt and offset the detachment, but Oligocene tuff, underlying older andesite, and the contact between these two units all dip shallowly to moderately east and west and are truncated by the underlying detachment.

For the most part, the detachment faults are highly disrupted by younger high-angle faults and/or overlapped and concealed beneath younger Cenozoic strata. In the southern Royston Hills (Fig. 16) the detachment fault, exposing upper Paleozoic rocks of the lower plate and about a 90 km^2 expanse of the upper-plate succession composed of Oligocene tuff, is preserved. Here, the upper-plate tuffs are cut by a system of west-northwest and north-south striking high-angle faults that do not penetrate the underlying detachment. The west-northwest trending faults form as single strands or anastomosing splays in a zone up to 1 km wide and have trace-lengths of up to 5 km . The north-south striking faults have trace-lengths of 1 km to 2 km and are subparallel to the strike of the tuffs. Displacement on the north-south trending structures resulted in 25° to 55° westward tilts of compaction foliation in the tuff units.

The Monte Cristo detachment is depositionally overlain and sealed by upper Miocene volcanic and sedimentary rocks. The 15 Ma Gilbert andesite rests depositionally on all Cenozoic rocks of the upper plate and also on the underlying Paleozoic and Mesozoic rocks. The underlying detachment was broadly folded in northwest-trending structures prior to deposition of the upper

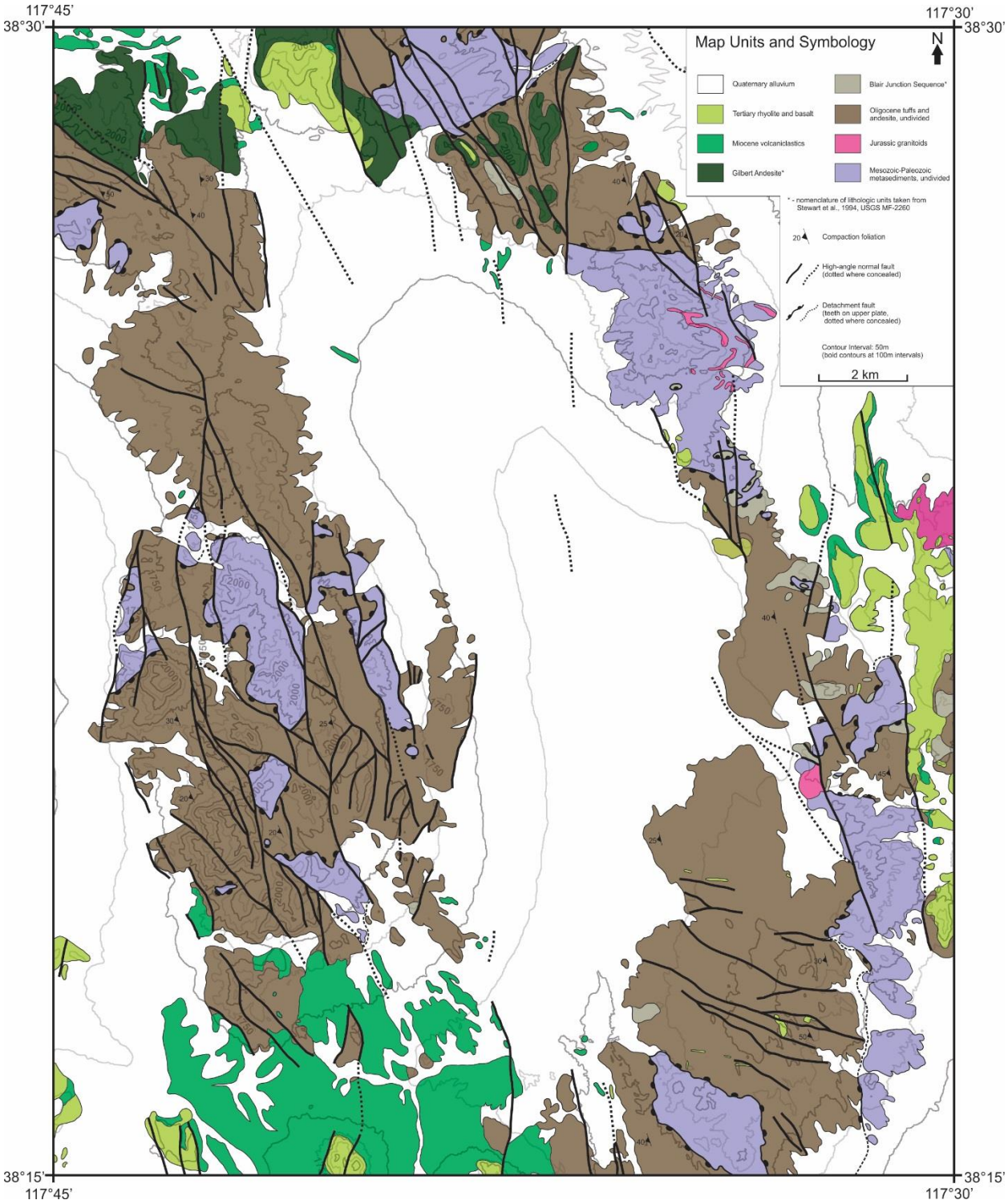

Figure 16. Geologic map of the Royston Hills and southern Cedar Mountains. Modified from Whitebread and Hardyman, 1987, USGS Open-File Report 87-613.

Miocene rocks. The mid-Miocene andesite and overlying sedimentary rocks were also broadly folded but with a lesser degree of limb appression than in older Cenozoic rocks, indicating that the underlying fold continued to grow during the late Miocene. The youngest layered rocks consisting of 7.2 Ma basalt, however, is flat-lying and was deposited after the cessation of shortening.

CHAPTER 6

STRUCTURE AND MINERALIZATION

Cenozoic structures of the central and southern Walker Lane and Mina deflection (Fig. 2) are responsible for the localization of epithermal gold-silver and the unroofing of older pluton related base-metal and orogenic gold deposits (Proffett, 1977; John, et al., 1989; Hardyman and Oldow, 1991; Raines et al.,1991; Oldow et al., 2003; Craig, 2003). The ages of pluton-related deposits are well established and range from Jurassic to Paleocene (Dilles and Wright, 1988; Harris, 1991; Shaver, 1991). Orogenic deposits, on the other hand, generally are poorly constrained as Jura-Cretaceous but locally, as in the SPLM extensional complex exposed at Mineral Ridge in the Silver Peak Range, have well constrained mineralization ages of between 90 to 80 Ma (Oldow et al., 2003). Exposure of older deposits is achieved by exhumation of footwall assemblages by late Cenozoic high-angle faults and locally by low-angle structures. Low-angle structures are formed generally in two ways. In areas such as the Yerington district (sensu lato) of western Nevada, they are formed by progressive horizontal-axis rotation (tilting) of faults that formed initially as high-angle structures (Proffett, 1977). Elsewhere, such as in the SPLM extensional complex, low-angle detachment structures are primary features formed with dips of less than 20° (Oldow et al., 1994). In these cases, localization of the mineralization pre-dates late Cenozoic structures, which only served to exhume or expose the older deposits. In contrast, widespread epithermal gold-silver deposits (Fig. 17) are spatially controlled by late Cenozoic structures in other areas (John et al., 1989; Hardyman and Oldow, 1991). Most of the deposits are found along high-angle fault systems (Fig. 17) with mineralization occurring

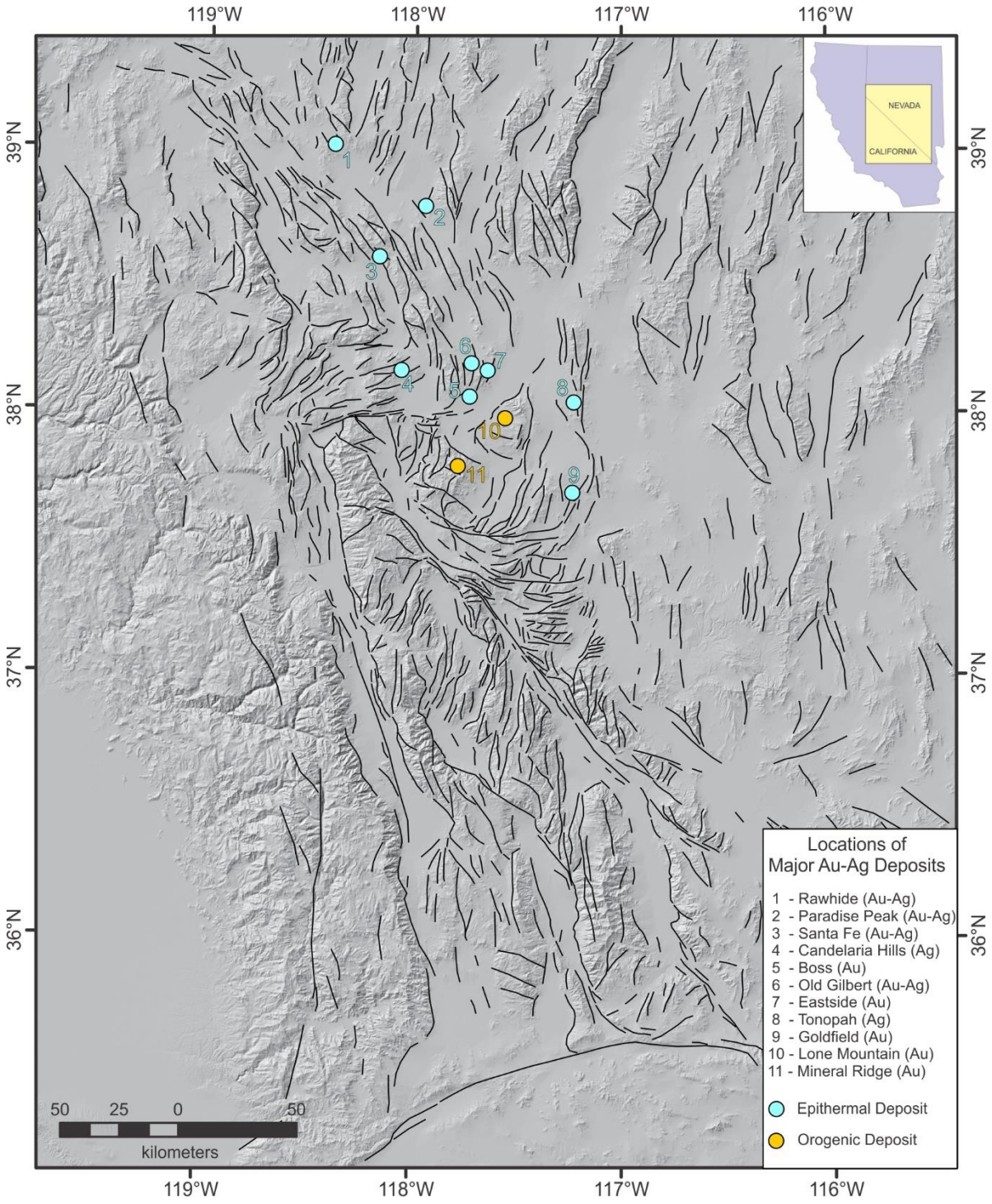

Figure 17. Locations of major gold-silver deposits in the southwestern Great Basin.

between 26 to 16 Ma (John et al., 1989, 1991; Black, 1991; du Bray et al., 2014), but some deposits, such as the Eastside district in the Monte Cristo Range, were formed after the deposition of late Miocene host rocks (Eng, 1991; Noble et al., 1991).

In most epithermal mineral districts, the deposits are attributed to formation within and along high-angle fault systems (John et al., 1989; Black et al., 1991), but low-angle faults are increasingly recognized as important mineralizing structures. The coeval development of high-angle and detachment faults (Hardyman and Oldow, 1991) and their role in ore-body geometry is well established in the Santa Fe (Fiannaca, 1983) and Paradise Peak (Sillitoe and Lorson, 1994) deposits, and may be important but unrecognized contributors to others deposits formed in similar structural settings such as Rawhide (Black et al., 1991). The Monte Cristo detachment in the eastern Mina deflection region is characterized by substantial cataclastic breccias showing evidence of hydrothermal alteration and mineralization in the lower-plate of the low-angle fault. The pervasive and regional extent of low-angle faults in the region underlying the eastern Mina deflection may provide the conditions for epithermal mineralization from displacement on or structural preparation by the detachment structures.

CHAPTER 7

DISCUSSION AND CONCLUSIONS

The region underlying the eastern part of the Mina deflection exposes a broad structural belt of active east-northeast striking left-oblique faults that curve into north-northwest striking right-oblique faults and are superposed onto a previously unrecognized and regionally extensive detachment fault system, named here as the Monte Cristo detachment. The detachment fault decoupled late Cenozoic volcanic and sedimentary rocks from underlying Paleozoic-Mesozoic layered rocks and Mesozoic plutonic rocks. The late Cenozoic rocks are divided into two lithologic successions separated by an angular unconformity. The lower lithologic section constitutes the upper-plate assemblage and consists of Oligocene ash-flow tuffs and andesite ranging from 29 to 24 Ma and an overlying Miocene succession of andesite lavas, lahar deposits, intrusive rocks, volcaniclastic sediments and tuff ranging from 22 to 17 Ma. In the northern Silver Peak and Monte Cristo Ranges, the northern Volcanic Hills, and the southern Cedar Mountains and Royston Hills, the Oligocene tuffs and Miocene andesite succession are everywhere found in direct structural contact with the pre-Cenozoic basement rocks and dip at moderate to steep angles back into the low-angle detachment fault. The upper Cenozoic succession consists of volcanic and volcaniclastic rocks ranging from 15 to about 7 Ma which seal the Monte Cristo detachment fault, sit in depositional contact with the basement rocks and overlie the lower Cenozoic section with angular unconformity. Timing constraints for activity on the Monte Cristo detachment are provided by the radiometric ages of the youngest Cenozoic rocks that sit in detachment contact versus the ages of the oldest Cenozoic rocks that sit in

depositional contact with the Paleozoic-Mesozoic basement. Based on the ages of the Cenozoic rocks and their relationship to the underlying basement rocks, movement on the Monte Cristo detachment is constrained from about 17 to 15 Ma.

The Monte Cristo detachment is situated within the upper-plate of and pre-dates the Silver Peak – Lone Mountain (SPLM) extensional complex, which was active from about 13 to 5 Ma. The SPLM detachment system separates a lower plate of lower amphibolite-facies metamorphic tectonites from an upper-plate assemblage of Paleozoic metasediments and late Cenozoic volcanic and sedimentary rocks. The Monte Cristo detachment subdivides the upper-plate assemblage of the SPLM extensional complex into an additional set of structural plates, decoupling the late Cenozoic rocks from the underlying Paleozoic basement. The Monte Cristo and SPLM detachment faults form a "double-detachment system" with an older, shallower detachment situated above a younger, deeper detachment, that is structurally analogous to the setting documented in the Bullfrog Hills by Maldonado, (1990), to the east of southern Death Valley. The Monte Cristo detachment is broadly folded in west-northwest and north-northeast to north-south trending, low-amplitude, long wavelength folds that developed contemporaneously with upper-plate transport and exhumation of metamorphic tectonites along the SPLM extensional complex.

The Monte Cristo detachment is pervasively cross-cut and offset by younger high-angle transcurrent and extensional faults of the Mina deflection by several tens to hundreds of meters. The detachment fault also truncates several older high-angle faults that are associated with an earlier generation of extensional faulting. Several places in the northern Silver Peak Range and Volcanic Hills demonstrate the presence of older, east-west and north-northeast striking high-

angle faults which juxtaposed different sections of Oligocene ash-flow tuff with highly variable thicknesses prior to the initiation of detachment faulting at about 17 Ma. The older generation of high-angle faults may have exerted structural control on the deposition of Oligocene to Miocene volcanic rocks, based on major thickness changes in upper plate rocks across faults which are truncated by the underlying detachment and do not penetrate into the basement.

Late Oligocene to early Miocene half-graben systems that controlled the deposition of Oligocene ash-flow tuffs and Miocene andesites are well documented in other parts of the region (Kerstetter, 2016a, 2016b), such as in the Candelaria Hills and the Miller Mountain area. Rocks of the lower Cenozoic stratigraphic succession exposed in the northern Silver Peak and Monte Cristo Ranges, northern Volcanic Hills, and Cedar Mountains and Royston Hills are highly disarticulated and structurally attenuated due to a protracted history of deformation on both high-angle and low-angle faults. It is possible that late Oligocene to early Miocene half-grabens were present in these areas and controlled the deposition of ash-flow tuff and andesite successions prior to the onset of detachment faulting at about 17 Ma. The geometry of speculative pre-detachment basins in the eastern Mina deflection cannot be directly observed or reconstructed due to extensive structural disarticulation and attenuation, however, and only inferred on a basis of major thickness changes in Oligocene to Miocene volcanic rocks across pre-detachment high-angle faults with similar orientations to those documented in age-equivalent half-graben systems further to the north and west.

Epithermal deposits attributed to formation within and along high-angle fault systems are well documented in the western Great Basin, but the presence of previously unrecognized low-

angle detachment faults might serve an important role as another type of mineralizing structure. The Monte Cristo detachment exposed across the eastern Mina deflection displays substantial cataclastic breccias and evidence of hydrothermal alteration in many places along the structural contact between Cenozoic and pre-Cenozoic rocks. The pervasive and regional extent of low-angle faults in the region underlying the eastern Mina deflection may provide the conditions for epithermal mineralization of gold-silver deposits from displacement on or structural preparation by the detachment structures, and may hold economic potential for new, previously unrecognized mineral exploration targets.

REFERENCES

Albers, J.P., and Stewart, J.H., 1972, Geology and mineral deposits of Esmeralda County, Nevada: Nevada Bureau of Mines and Geology, Bulletin 78, 80 p.

Argus, D.F., and Gordon, R.G., 1991, Current Sierra Nevada – North America motion from very long baseline interferometry: Implications for the kinematics of the western United States: Geology, v. 19, p. 1,085-1,088.

Bachman, S.B., 1978, Pliocene-Pleistocene break-up of the Sierra Nevada-White-Inyo Mountains block and formation of the Owens Valley: Geology, v. 6, p. 461-463.

Bennett, R.A., Davis, J.L., and Wernicke, B.P., 1999, Present-day pattern of Cordillera deformation in the western United States: Geology, v., 27, p. 371-374.

Bidgoli, T.S., Amir, E, Walker. J.D., Stockli, D.F., Andrew, J.E., and Caskey, S.J., 2015, Low-temperature thermochronology of the Black and Panamint Mountains, Death Valley, California: Implications for geodynamic controls on Cenozoic intraplate strain: Lithosphere, v. 7, p. 473-480; doi: 10.1120/L406.1

Black, J.E., Mancuso, T.K, and Gant, J.L., 1991, Geology and mineralization at the Rawhide Au-Ag deposit, Mineral County, Nevada, in Raines, G.L., ed., Geology and Ore Deposits of the Great Basin: Reno, Geological Society of Nevada, p. 1123-1144.

Burchfiel, B. C., and Stewart, J. H., 1966, "Pull-apart" origin of the central segment of Death Valley, California: Geological Society of America Bulletin, v. 77, p. 439-442.

Burchfiel, B.C., Hodges, K.V., and Royden, L.H., 1987, Geology of Panamint Valley – Saline Valley pull-apart system, California: Palinspastic evidence for low-angle geometry of a Neogene range-bounding fault: Journal of Geophysical Research, v. 92, p. 10,422-10,426.

Burchfiel, B. C., Cowan, D. S., and Davis, G. A., 1992, Tectonic overview of the Cordilleran orogen in the western United States, *in* Burchfiel, B. C., Lipman, P. W., and Zoback, M. L., editors., The Cordilleran Orogen: Conterminous U. S.: Geological Society of America, The Geology of North America, v. G-3, p. 407-480.

Cland, B., and Oldow, J.S., 2017, Late Cenozoic superposition of high-angle faults and low-angle detachment faults in the eastern Mina deflection, west-central Nevada: Geological Society of America Abstracts with Programs, v. 49, no 6, session 385-25.

Conrad, J.E., 1993, Late Cenozoic tectonics of the southern Inyo Mountains, eastern California: M.S. thesis, San Jose State University, 84 p.

Craig, S.D., 2003, Geology and gold mineralization of the Mineral Ridge gold mine, Esmeralda County, Nevada: Geological Society of Nevada; Special Publication 38, Regional Geology and Gold Deposits in the Sliver Peak Area, Mineralization Hosted by Metamorphic Core Complexes, p. 81-106.

Diamond, D.S., and Ingersoll, R.A., 2002, Structural and sedimentologic evolution of a Miocene supradetachment basin, Silver Peak Range and adjacent areas, west-central Nevada: International Geology Review, v. 44, p. 588-623

Dilles, J. H., and Wright, J.E., 1988, The chronology of early Mesozoic arc magmatism in the Yerington district of western Nevada and its regional implications: Geological Society of America Bulletin, v. 100, p. 644-652.

Dilles, J.H., and Gans, P.B., 1995, The chronology of Cenozoic volcanism and deformation in the Yerington area, western Basin and Range and Walker Lane, Geological Society of America Bulletin, v. 107, p. 474-486.

Dixon, T.H., Miller, M., Farina, F., Wang, H., and Johnson, D., 2000, Present-day motion of the Sierra Nevada block and some tectonic implications for the Basin and Range Province, North American Cordillera: Tectonics, v. 19, p. 1-24.

Dokka, R.K., and Travis, C.J., 1990, Role of the Eastern California shear zone in accommodating Pacific-North American plate motion: Geophysical Research Letters, v. 17, p. 1323-1326.

du Bray, E.A., John, D.A., and Cousens, B.L., 2014, Petrologic, tectonic, and metallogenic evolution of the southern segment of the ancestral Cascades magmatic arc, California and Nevada: Geosphere, v. 10, p. 1-39; doi: 10.1130/GES009441.1

Ekren, E.B., Byers, F.M., Jr., Hardyman, R.F., Marvin, R.F., Silberman, M.L., 1980, Stratigraphy, preliminary petrology, and some structural features of Tertiary volcanic rocks in the Gabbs Valley and Gillis ranges, Mineral County, Nevada: U. S. Geological Survey Bulletin, B 1464, p. 54.

Elison, M.W., Speed, R.C., and Kistler, R.W., 1990, Geologic and isotopic constraints on the crustal structure of the northern Great Basin: Geological Society of America Bulletin, v. 102, p. 1077-1092.

Eng, T., 1991, Geology and mineralization of the Freedom Flats gold deposit, Borealis mine, Mineral County, Nevada, in Raines, G.L., ed., Geology and Ore Deposits of the Great Basin: Reno, Geological Society of Nevada, p. 995-1019.

Evernden, J.F, and James, G.T., 1964, Potassium-Argon dates and the Tertiary floras of North America: American Journal of Science, v. 262, p. 945-974.

Ferranti, L., Oldow, J.S., Geissman, J.W., and Nell, M.M., 2009, Coordinated displacement and finite flattening on linked arrays of curved faults, Rhodes Salt Marsh basin, central Walker Lane belt, Nevada, *in* Oldow, J.S., and Cashman, P.H, eds, Late Cenozoic Structure and Evolution of the Great Basin –Sierra Nevada Transition: Geological Society of America Special Paper 447, p. 189-214.

Fiannaca, M., 1983, Geology of the Santa Fe gold-silver deposits, Mineral County, Nevada: Geological Society of Nevada Bulk Mineable Precious-Metal Deposits of the Western United States Symposium, Reno, Nevada, 1987, Guidebook for field trips, p. 233-239.

Frankel, K.L., Glazner, A.F., Kirby, E., Monastero, F.C., Strane, M.D., Oskin, M.E., Unruh, J.R., Walker, J.D., Anandakrishnan, S., Bartley, J.M., Coleman, D.S., Dolan, J.F., Finkel, R.C., Greene, D., Kylander-Clark, A., Morrero, S., Owen, L.A., and Phillips, F., 2008, Active tectonics of the eastern California shear zone, in Duebendorfer, E.M., and Smith, E.I., eds., Field Guide to Plutons, Volcanoes, Faults, Reefs, Dinosaurs, and Possible Glaciation in Selected Areas of Arizona, California, and Nevada: Geological Society of America Field Guide 11, p. 43–81, doi: 10.1130/2008.fl d011(03).

Ferguson, H.G., Muller, S.W., and Cathcart, S.H., 1953, Geology of the Coaldale quadrangle, Nevada: U.S. Geological Survey Geologic Quadrangle Map, map scale 1:100,000, GQ-23.

Garside, L.J., 1979, Geologic map of the Camp Douglas quadrangle, Nevada: Nevada Bureau of Mines and Geology, Map 63, scale 1:24,000.

Guest, B., Niemi, N., and Wernicke, B., 2007, Stateline fault system: A new component of the Miocene-Quaternary eastern California shear zone: Geological Society of America Bulletin, v. 119, p. 1337-1346.

Hambrick, D.A., 1984, Geochemistry and structure of the Tertiary volcanic rocks in the southern Monte Cristo Range, Nevada: M.S. thesis, University of Arizona, 140 p.

Hardyman, R.F., and Oldow, J.S., 1991, Tertiary tectonic framework and Cenozoic history of the central Walker Lane, Nevada, in Raines, G.L., ed., Geology and Ore Deposits of the Great Basin: Reno, Geological Society of Nevada, p. 279-302.

Hoeft, J.S., and Frankel, K.L., 2010, Temporal variations in extension rate of the Lone Mountain fault and strain distribution in the eastern California shear zone – Walker Lane: Geosphere, v. 6, p. 917-936; doi: 10.1130/GES00603.1

Hodges, K.V., McKenna, L.W., and Harding, M.B., 1990, Structural unroofing of the central Panamint Mountains, Death Valley region, southeastern California, in Wernicke, B.P., ed., Basin and Range extensional tectonics near the latitude of Las Vegas, Nevada: Boulder, Colorado, Geological Society of America Memoir 176, p. 337-390.

Hoisch, R.D., and Simpson, C., 1993, Rise and tilt of the metamorphic rocks in the lower plate of a detachment fault in the Funeral Mountains, Death Valley, California: Journal of Geophysical Research, v. 98 p. 6805-6827.

Hoisch, T.D., Heizler, M.T., and Zartman, R.E., 1997, Timing of detachment faulting in the Bullfrog Hills and Bare Mountain area, southwest Nevada: Inferences from 40Ar/39Ar, K-Ar, P-Pb, and fission track thermochronology: Journal of Geophysical Research, v. 102, B2, p. 2815-2833.

Holm, D.K., and Wernicke, B., 1990, Black Mountains crustal section, Death Valley extended terrain, California: Geology, v. 18, p. 520-523.

Holm, D.K., and Dokka, R.K., 1993, Interpretation and tectonic implications of cooling histories: An example from the Black Mountains, Death Valley extended terrane, California: Earth and Planetary Science Letters, v. 116, p. 63-80.

Hulen, J. B., Nash, G.D., and Deymonaz, J., 2005, DOE enables the Emigrant geothermal exploration and slimhole drilling project in Fish Lake Valley, Nevada: Geothermal Research Council Bulletin, p. 176-183.

John, D.A., 1987, Map showing the distribution and characteristics of plutonic rocks in the Tonopah 1° by 2° quadrangle, central Nevada: United States Geological Survey Miscellaneous Field Studies Map MF-1877-J, scale 1:250,000.

John, D.A., 1992, Stratigraphy, regional distribution, and reconnaissance geochemistry of Oligocene and Miocene volcanic rocks in the Paradise Range and northern Pactolus Hills, Nye County, Nevada: United States Geological Survey Bulleting 1974, 67 p.

John, D.A., 2001, Miocene and early Pliocene epithermal gold-silver deposits in the northern Great Basin, western United States: Characteristics, distribution, and relationship to magmatism: Economic Geology, v. 96, p. 1827-1853.

John, D.A., and Robinson, A.C.,1989, Rb-Sr whole-rock isotopic ages from granitic plutons in the western part of the Tonopah 1° by 2° quadrangle, Nevada: Isochron/West, no. 53, p. 20-27.

John, D.A., Thomason, R.E., and McKee, E.H., 1989, Geology and K-Ar geochronology of the Paradise Peak mine and the relationship of pre-Basin and Range extension to early Miocene precious metal mineralization in west-central Nevada: Economic Geology, v. 84, p.631-649.

John, D.A., Nash, J.J., Clark, C.W., and Wulftange, W.H., 1991, Geology, hydrothermal alteration, and mineralization at the Paradise Peak gold-silver-mercury deposit, Nye County, Nevada, in Raines, G.L., ed., Geology and Ore Deposits of the Great Basin: Reno, Geological Society of Nevada, p. 1020-1050.

Johnson, J.E., and Pendergast, A., 1981, Timing and mode of emplacement of the Roberts Mountain allochthon, Antler orogeny: Geological Society of America Bulletin, v. 92, 648-658.

Kerstetter, S.R., Oldow, J.S., and Katopody, D.T., 2016a, Mid-Miocene synextensional deposition during north-south extension in a west-northwest trending half graben in the western Great Basin: Geological Society of America Abstracts with Programs, v. 48, no. 4, 12-4.

Kerstetter, S.R., Katopody, D.T., and Oldow, J.S., 2016b, Architecture, kinematics, and development of widespread late Oligocene to early Miocene east-northeast and west-northwest trending extensional basins during north-south extension in the central and southern Walker Lane, western Great Basin: American Geophysical Union Abstract T41E-2974.

Kerstetter, S.R., and Oldow, J.S., 2016, Synorogenic deposition in an east-northeast trending half graben during late Oligocene to mid-Miocene north-south extension in west-central Nevada: Geological Society of America Abstracts with Programs, v. 48, no. 7, 274-7.

Kistler, R.W., 1978, Mesozoic paleogeography of California: A viewpoint from isotope geology, in Howell, D.G., and McDougall, K.A., eds., Mesozoic paleogeography of the western United States: Pacific Section, Society of Economic Paleontologists and Mineralogists, Pacific Coast Paleogeography Symposium 2, p. 107-110.

Kistler, R.W., and Peterman, Z.E., 1978, A study of the regional variations of initial strontium isotopic composition of Mesozoic granitic rocks in California: United States Geological Survey Professional Paper 1071, 17 p.

Lee, J., Stockli, D., Schroeder, J., Tincher, C., Bradley, D., and Owen, L., 2003, Fault slip transfer in the Eastern California Shear Zone and Walker Lane, in Lee, J., Stockli, D., Henry, C., and Dixon, T., conveners, Penrose Conference: Kinematics and Geodynamics of Intraplate Dextral Shear in Eastern California and Western Nevada, Boulder, Colorado, Geological Society of America, p. 22-44.

Lee, J., Stockli, D.F., Owen, L.A., Finkel, R.C., and Kislitsyn, R., 2009a, Exhumation of the Inyo Mountains, California: Implications for the timing of extension along the western boundary of the Basin and Range Province and distribution of dextral fault slip rates across the eastern California shear zone. Tectonics, v. 28, TC1001, doi:10.1029/2008TC002295

Lee, J., Garwood, J., Stockli, D.F., and Gosse, J., 2009b, Quaternary faulting in Queen Valley, California-Nevada: Kinematics of Fault Slip Transfer in the Eastern California Shear Zone-Walker Lane Belt. Geological Society of America Bulletin, v. 121, p. 599-614.

Lueddecke, S.B., Pinter, N., and Gans, P., 1998, Pliocene-Pleistocene ash falls, sedimentation, and range-front faulting along the White-Inyo Mountains front, California: Journal of Geology, v. 106, p. 511-522; doi: 10.1086/516038.

Mahan, K.H., Guest, B., Wernicke, B., and Niemi, N.A., 2009, Low-temperature thermochronologic constraints on the kinematic history and spatial extent of the Eastern California shear zone: Geosphere, v. 5, p. 483-495; doi: 10.1130/GES00226.1

Maldonado, F., 1990, Structural geology of the upper plate of the Bullfrog Hills detachment fault system, southern Nevada: Geological Society of America Bulletin, v. 102, p. 992-1006.

McKee, E.H., 1968, Age and rate of movement on the northern part of the Death Valley –Furnace Creek fault zone, California: Geological Society of America Bulletin, v. 79, p. 509-512.

McKee, E.H., and John, D.A., 1987, Map showing the location of samples used and K-Ar dating of Cenozoic rocks and minerals in the Tonopah 1° by 2° quadrangle, central Nevada: United States Geological Survey Miscellaneous Field Studies Map MF-1877-I, scale 1:250,000.

Miller, M.B., and Pavlis, T.L., 2005, The Black Mountains turtlebacks: Rosetta stones of Death Valley tectonics: Earth-Science Reviews, v. 73, p. 115-138

Moore, S.W., 1981, Geology of a part of the southern Monte Cristo Range, Esmeralda County, Nevada: M.S. thesis, San Jose State University, 157 p.

Mueller, N., Oldow, J.S., Katopody, D.T., Gibson, K., Pham, B., McBride, K., Shilpakar, P., and Aguilar, R., 2016a, Pliocene reorganization of the Eastern California Shear Zone kinematics documented in the Cucomungo Canyon restraining bend of the Furnace Creek – Fish Lake Valley fault zone, northern Death Valley and southern Fish Lake Valley, California: Geological Society of America Abstracts and Programs, v. 48, no. 4, 1-3.

Mueller, N., Kerstetter, S.R., Katopody, D.T., and Oldow, J.S., 2016b, Subsurface constraints on late Cenozoic basin geometry in northern Fish Lake Valley and displacement transfer along the northern Fish Lake Valley fault zone, western Nevada: American Geophysical Union Abstract T41E-2975.

Mueller, N.J., and Oldow, J.S., 2017, Pliocene changes in kinematics and long-term geologic slip rates along the Furnace Creek – Fish Lake Valley fault zone, California and Nevada: Geological Society of America Abstracts with Programs, v. 49, no 6, 385-21.

Nagorsen-Rinke, S, Lee, J., and Calvert, A., 2013, Pliocene sinistral slip across the Adobe Hills, eastern California – western Nevada: Kinematics of fault slip transfer across the Mina deflection: Geosphere, v. 9, p. 37-55; doi: 10.1130/GES00825.1.

Niemi, N.A., 2012, Geologic map of the central Grapevine Mountains, Inyo County, California, and Esmeralda and Nye Counties, Nevada: Geological Society of America Digital Map and Chart Series 12, doi: 10.1130/2012.DMCH012.; doi: 10.1016/j.earscirev.2005.04.007.

Niemi, N.A., Wernicke, B.P., Brady, R.J., Saleeby, J.B., and Dunne, G.C., 2001, Distribution and provenance of the middle Miocene Eagle Mountain Formation, and implications for regional kinematic analysis of the Basin and Range Province: Geological Society of America Bulletin, v.113, p. 419-442.

Niemi, N.A., Wernicke, B.P., Friedrich, A. M., Simons, M., Davis, J.L., 2004, BARGEN continuous GPS data across the eastern Basin and Range Province, and implications for fault systems dynamics, Geophysical Journal International, v. 159, p. 842-862.

Noble, D.C., Weiss, S.I., and McKee, E.H., 1991, Magmatic and hydrothermal activity, caldera geology, and regional extension in the western part of the southwestern Nevada volcanic field, in Raines, G.L., ed., Geology and Ore Deposits of the Great Basin: Reno, Geological Society of Nevada, p. 913-934.

Oldow, J. S., 1981, Structure and stratigraphy of the Luning allochthon and the kinematics of allochthon emplacement, Pilot Mountains, west-central Nevada: Geological Society of America Bulletin, Part 1, v. 92, p. 888-911; Part 11. v. 92, p. 647-1669.

Oldow, J.S., 1983, Tectonic implications of a late Mesozoic fold and thrust belt in northwestern Nevada: Geology, v. 11, p. 542-546.

Oldow, J.S., 1984, Evolution of a late Mesozoic back-arc fold and thrust belt, western Great Basin, USA: Tectonophysics, v. 102, p. 245-274.

Oldow, J.S., 1984, Spatial variability in the structure of the Roberts Mountains allochthon, western Nevada: Geological Society of America Bulletin, v. 95, p. 174-185.

Oldow, J.S., 1992, Late Cenozoic displacement partitioning in the northwestern Great Basin, in Craig, S.D., editor., Structure, tectonics, and mineralization of the Walker Lane, Volume Walker Lane Symposium Proceedings Volume: Reno, Nevada, Geological Society of Nevada, p. 17-52.

Oldow, J.S., 2003, Active transtensional boundary zone between the western Great Basin and Sierra Nevada block, western US Cordillera: Geology, v. 31, p. 1033-1036.

Oldow, J.S., Bally, A.W., Ave Lallemant, H.G., and Leeman, W.P., 1989, Phanerozoic evolution of the North American Cordillera (United States and Canada), in Bally, A.W., and Palmer, A.R., editors., The Geology of North America: An overview, Volume A: Boulder, Colorado, Geological Society of America, Geology of North America, p. 139-232.

Oldow, J.S., Satterfield, J.I., and Silberling, N.J., 1993, Jurassic to Cretaceous transpressional deformation in the Mesozoic marine province of the northwestern Great Basin, in Lahren, M.M., Trexler, J.H., and Spinosa, C., Crustal Evolution of the Great Basin and the Sierra Nevada, Geological Society of America Field Trip Guidebook, p. 129-166.

Oldow, J.S., Kohler, G., and Donelick, R.A., 1994, Late Cenozoic extensional transfer in the Walker Lane strike-slip belt, Nevada: Geology, v. 22, p. 637-640.

Oldow, J.S., Payne, J.D., Prestia, V.I., McClelland, W.C., and Ferranti, L., 2003, Stratigraphic and structural evolution of the Silver Peak extensional complex, western Great Basin, USA: Geological Society of Nevada; Special Publication 38, Regional Geology and Gold Deposits in the Silver Peak Area, Mineralization Hosted by Metamorphic Core Complexes, p. 51-78.

Oldow, J.S., Geissman, J.W., and Stockli, D.F., 2008, Evolution and strain reorganization within late Neogene structural stepovers linking the central Walker Lane and northern Eastern California Shear Zone, western Great Basin, International Geology Review v. 50, p. 270-290.

Oldow, J.S., Elias, E.A., Ferranti, L., McClelland, W.C., and McIntosh, W.C., 2009, Late Miocene to Pliocene synextensional deposition in fault-bounded basins within the upper plate of the western Silver Peak – Lone Mountain extensional complex, west-central Nevada, *in* Oldow, J.S. and Cashman, P.H., eds., Late Cenozoic Evolution of the Western Great Basin, Geological Society of America Special Paper 447, p.275-312.

Oldow, J.S., and Geissman, J.W., 2013, Evolution of a late Miocene to contemporary displacement transfer system between the northern Furnace Creek and southern Fish Lake Valley fault zones and the central Walker Lane, southwest Nevada: Geological Society of America Abstracts with Programs, v. 45, no. 7, 85-5.

Petronis, M.S., Geissman, J.W., Oldow, J.S., and McIntosh, W.C., 2002, Paleomagnetic and $^{40}Ar/^{39}Ar$ geochronologic data bearing on the structural evolution of the Silver Peak Range, west-central Nevada: Geological Society of America Bulletin v. 114, p. 1108-1130.

Petronis, M.S., and Geissman, J.W., 2008, Anisotropy of magnetic susceptibility data bearing on the transport direction of mid-Tertiary regional ignimbrites, Candelaria Hills area, west-central Nevada: Bulletin of Volcanology v. 71, p. 121-151.

Petronis, M.S., Geissman, J.W., Oldow, J.S., and McIntosh, W.C., 2009, Neogene vertical-axis rotation and development of the Mina deflection, central Walker Lane, Nevada, *in* Oldow, J.S., and Cashman, P.H, eds, Late Cenozoic Structure and Evolution of the Great Basin –Sierra Nevada Transition: Geological Society of America Special Paper 447, p. 215-254.

Proffett, J.M., 1977, Cenozoic geology of the Yerington district, Nevada, and implications for the nature and origin of Basin and Range faulting: Geological Society of America Bulletin, v 88, p 247-266.

Proffett, J.M, and Dilles, J.H., 1984, Geologic map of the Yerington district, Nevada: Nevada Bureau of Mines and Geology, Map 77.

Raines, G.L., Lisle, R.E., Schafer, R.W., and Wilkinson, W.H., 1991, Geology and ore deposits of the Great Basin: Geological Society of Nevada Symposium, 1257 p.

Reheis, M.C., 1991, Geologic map of Late Cenozoic deposits and faults in the western part of the Rhyolite Ridge 15 minute Quadrangle, Esmeralda County, Nevada: U.S. Geological Survey, Miscellaneous Investigations Series, Map I-2183, scale: 1:24,000.

Reheis, M.C., Slate, J.L., Sarna-Wojcicki, A.M., and Meyer, C.E., 1993, A late Pliocene to middle Pleistocene pluvial lake in Fish Lake Valley, Nevada and California: Geological Society of American Bulletin, v. 105, p. 953-967.

Reheis, M.C., and Dixon, T.H., 1996, Kinematics of the eastern California shear zone: Evidence for slip transfer from Owens and Saline Valley fault zones to Fish Lake Valley fault zone: Geology, v. 24, p. 575-575.

Reheis, M. C., and Sawyer, T. L., 1997, Late Cenozoic history and slip rates of the Fish Lake Valley, Emigrant Peak, and Deep Springs fault zones, Nevada and California: Geological Society of America Bulletin, v. 109, p. 280-299.

Roberts, R.J., Hotz, P.E., Gilluly, J., and Ferguson, H.G., 1958, Paleozoic rocks of north-central Nevada: American Association of Petroleum Geologists, v. 42, p. 2813-2857.

Robinson, P. T., McKee, E. H. and Moiola, R. J., 1968, Cenozoic volcanism and sedimentation, Silver Peak region, western Nevada and adjacent California, *in* Coats, R. R., Hay, R. L. and Anderson, C., Studies in Volcanology: Geological Society of America Memoir 116, p. 577-612.

Robinson, P.T., and Crowder, D. F., 1973, Geologic map of the Davis Mountain quadrangle, Esmeralda and Mineral Counties, Nevada: U. S. Geological Survey, map scale 1:62,500, GQ-1078.

Robinson, P. T., Stewart, J. H., Moiola, R. J. and Albers, J. P., 1976, Geologic map of the Rhyolite Ridge quadrangle, Esmeralda County, Nevada: U. S. Geological Survey, map scale 1:62,500, GQ-1325.

Ross, D. C., 1961, Geology and mineral deposits of Mineral County, Nevada: Nevada Bureau of Mines and Geology, Bulletin 58, 98 p.

Ryall, A., and Priestley, K., 1975, Seismicity, secular strain, and maximum magnitude in the Excelsior Mountains area, western Nevada and eastern California: Geological Society of America Bulletin, v. 86, p. 1585-1592.

Saleeby, J.B., 1986, C-2 central California offshore to Colorado Plateau: Boulder, Colorado, Geological Society of America Centennial Continent/Ocean Transect #10.

Sarna-Wojcicki, A.M., Reheis, M.C., Pringle, M.S., Fleck, R.J., Burbank, D., Meyer, C.E., Slate, J.L., Wan, E., Budahn, J.R., Troxel, B., and Walker, J.P., 2005, Tephra layers of Blind Spring Valley and related upper Pliocene and Pleistocene tephra layers, California, Nevada, and Utah: Isotopic ages, correlation, and magnetostratigraphy: United States Geological Survey, Professional Paper 1701, 59 p.

Serpa, L., and Pavlis, T.L., 1996, Three dimensional model of the Cenozoic history of the Death Valley region, southeastern California: Tectonics, v. 15, p. 1113-1128.

Schweickert, R.A., and Lahren, M.M., 1997, Strike-slip fault system in the Amargosa Valley and Yucca Mountain, Nevada: Tectonophysics, v. 272, p. 25-41, doi: 10.1016/S0040-1951(96)00274-0.

Shaver, S.A., 1991, Geology, alteration, mineralization, and trace element geochemistry of the Hall (Nevada Moly) deposit, Nye County, Nevada, in Raines, G.L., ed., Geology and Ore Deposits of the Great Basin: Reno, Geological Society of Nevada, p. 303-332.

Shaver, S.A., and McWilliams, M., 1987, Cenozoic extension and tilting recorded by Upper Cretaceous and Tertiary rocks at the Hall molybdenum deposit, northern San Antonio Mountains, Nevada: Geological Society of America Bulletin, v. 99, p. 341-353.

Sillitoe, R.H., and Lorson, R.C., 1994, Epithermal gold-silver-mercury deposits at Paradise Peak, Nevada: Ore controls, porphyry gold association, detachment faulting, and supergene oxidation: Economic Geology, v. 89, p. 1228-1248.

Snow, J., and Wernicke, B., 2000, Cenozoic tectonism in the central basin and range: Magnitude, rate, and distribution of upper crustal strain: American Journal of Science, v. 300, p. 659-719.

Speed, R.C., 1977, Excelsior Formation, west central Nevada: Stratigraphic appraisal, new divisions, and Paleogeographic interpretations, Stewart, J.H., Stevens, C.H., and Fritsche, A.E., eds, Paleozoic Paleogeography of the Western United States: Pacific Coast Paleogeography Symposium 1:, p. 325-336.

Speed, R.C., 1978, Paleogeographic and plate tectonic evolution of the early Mesozoic marine province of the western Great Basin, *in* Howell, D. G., McDougall, K., eds., Mesozoic Paleogeography of the Western United States: Pacific Coast Paleogeography Symposium (2), p. 253-270.

Speed, R.C., 1979, Collided Paleozoic microplate in the western United States: Journal of Geology, v. 87, p. 279-292.

Speed, R.C., 1984, Paleozoic and Mesozoic continental margin collision zone features: Mina to Candelaria, Nevada, traverse (field trip 6), in Lintz, J., ed. Western Geological Excursions: Geological Society of America, Annual Meeting, Reno, Nevada, v.4, p. 66-80.

Speed, R.C. and Cogbill, A.H., 1979, Cenozoic volcanism of the Candelaria region, Nevada, Geological Society of America Bulletin, Part II, v. 90, p. 456-493.

Speed, R. C., and Sleep, N. H., 1982, Antler Orogeny and foreland basin; a model: Geological Society of America Bulletin, v. 93, p. 815-828.

Sternlof, K.R., 1988, Structural style and kinematic history of the active Panamint-Saline extensional system, Inyo County, California: M.S. thesis, Massachusetts Institute of Technology, 30 p.

Stewart, J.H., 1967, Possible large right-lateral displacement along fault and shear zones in the Death Valley-Las Vegas areas, California and Nevada: Geological Society of America Bulletin, v. 78, p. 131-142.

Stewart, J.H., 1980, Geology of Nevada: Nevada Bureau of Mines and Geology Special Publication 4, 136 p.

Stewart, J.H., 1983, Extensional tectonics in the Death Valley area, California: Transport of the Panamint Range structural block 80 km northwestward: Geology, v. 11, p. 153-157.

Stewart, J.H., 1988, Tectonics of the Walker Lane belt, western Great Basin: Mesozoic and Cenozoic deformation in a shear zone, in Ernst, W.G., ed., Metamorphism and crustal evolution of the western United States: Englewood Cliffs, New Jersey, Prentice-Hall, p. 681-713.

Stewart, J.H., 1989; Description, stratigraphic sections, and maps of middle and upper Miocene Esmeralda Formation in Alum, Blanco mine, and Coaldale areas, Esmeralda County, Nevada: United States Geological Survey, Open-File Report 98-324.

Stewart, J. H., Albers, J.P., and Poole, F.G., 1968, Summary of regional evidence for right-lateral displacement in the western Great Basin: Geological Society of America Bulletin, v. 79, p. 1407-1414.

Stewart, J. H. and Diamond, D. S., 1990, Changing patterns of extensional tectonics; overprinting of the basin of the middle and upper Miocene Esmeralda Formation in western Nevada by younger structural basins, *in* Wernicke, B. P., ed., Basin and Range extensional tectonics near the latitude of Las Vegas, Nevada: Boulder, Colorado, Geological Society of America Memoir 176.

Stewart, J.H., Kelleher, P.C., and Zorich, E.A., 1994, Geologic map of the Monte Cristo Range area, Esmeralda and Mineral Counties, Nevada: U.S. Geological Survey Map MF-2260 scale 1:62,500.

Stockli, D.F., Dumitru, T.A., McWilliams, M.O., and Farley, K.A., 2003, Cenozoic Tectonic Evolution of the White Mountains, California and Nevada. Geological Society of America Bulletin, v. 115, p. 788-816.

Tincher., C.R., and Stockli, D.F., 2009, Cenozoic volcanism and tectonics in the Queen Valley Area, Esmeralda County, Western Nevada, *in* Oldow, J.S., and Cashman, P.H., eds., Late Cenozoic Evolution of the Western Great Basin, GSA Special Paper 447, p. 255-274.

Wallace, R.E., 1984, Patterns and timing of late Quaternary faulting in the Great Basin Province and relation to some regional tectonic features: Journal of Geophysical Research, v. 89, p. 5,763-5,769.

Whitebread, D.H, and Hardyman, R.F., 1987, Preliminary geologic map of part of the Cedar Mountains and Royston Hills, Esmeralda and Nye Counties, Nevada: United States Geological Survey, Open-File Report 87-613.

Worthington, J.E., 1992, Neogene structural and volcanic geology of the Gold Mountains – Slate Ridge area, Esmeralda County, Nevada: M.S. thesis, University of Nevada, Reno, 75 p.

BIOGRAPHICAL SKETCH

Brent Cland was born in Brooklyn, New York in 1993 and moved to Dallas, Texas in 2007. Brent earned a Bachelor of Science in Geosciences from The University of Texas at Dallas in Spring 2015. Brent fast-tracked into the Master's program at UT Dallas and began his graduate studies and thesis work in structural geology and geologic mapping under the advisement of Dr. John Oldow in Summer 2015. Brent was part of a collaborative and multidisciplinary research team of graduate students known as the Ellison Miles Center for Geological Field Studies directed by Dr. Oldow, whose focus was to build an integrated regional framework and better understanding of the structural systems operating in the Eastern California shear zone and central Walker Lane region of west-central Nevada.

CURRICULUM VITAE

Brent Cland

800 W Campbell Rd, Richardson TX, 75080
University of Texas at Dallas, Department of Geosciences, ROC 21

Education

Master of Science (M.S.) in Geosciences
The University of Texas at Dallas
Summer 2015 – Summer 2017
GPA: 4.000

Bachelor of Science (B.S.) in Geosciences
The University of Texas at Dallas
Fall 2011 – Spring 2015
GPA: 3.428

Awards

"Highest Achievement in Geosciences," Outstanding Senior Award, Fall 2014

Research and Experience

Graduate Research Assistant, UT Dallas, Dept. of Geosciences
Summer 2015 – Summer 2016

Graduate Teaching Assistant, UT Dallas, Dept. of Geosciences
Fall 2014 – Spring 2016

Field Geology Assistant, UT Dallas, Dept. of Geosciences
Summer 2014: Fish Lake Valley, NV
Summer 2015: San Juan Islands, WA

Abstracts

Cland, B., and Oldow, J.S., 2017, Late Cenozoic superposition of high-angle faults and low-angle detachment faults in the eastern Mina deflection, west-central Nevada: Geological Society of America Abstracts with Programs, v. 49, no 6, session 385-25.